Article:
Gao, H, Boillat, A, Huang, D et al. (2017) Intracellular Zinc Activates KCNQ Channels by Reducing their Dependence on Phosphatidylinositol 4,5-bisphosphate. Proceedings of the National Academy of Sciences, 114 (31). E6410-E6419. ISSN: 0027-8424

https://doi.org/10.1073/pnas.1620598114

BIOLOGICAL SCIENCE: Neuroscience

Intracellular Zinc Activates KCNQ Channels by Reducing their Dependence on Phosphatidylinositol 4,5-bisphosphate

Haixia Gao[a,b], Aurélien Boillat[a], Dongyang Huang[b], Ce Liang[b], Chris Peers[c], Nikita Gamper[a,b]*

[a]Faculty of Biological Sciences, University of Leeds, Leeds, UK
[b]Department of Pharmacology, Hebei Medical University, Shijiazhuang, China
[c]LICAMM, Faculty of Medicine and Health, University of Leeds, Leeds, UK

*Correspondence should be sent to

Nikita Gamper
School of Biomedical Sciences
Faculty of Biological Sciences
University of Leeds
Leeds, UK
Tel: +44 (0)113 343 7923
Email: n.gamper@leeds.ac.uk

Keywords: M channel/KCNQ/Kv7/Zinc/ Phosphatidylinositol 4,5-bisphosphate

Abstract

M-type (Kv7, KCNQ) potassium channels are proteins that control excitability of neurons and muscle cells. Many physiological and pathological mechanisms of excitation operate via the suppression of M channel activity or expression. Conversely, pharmacological augmentation of M channel activity is a recognized strategy for treatment of hyperexcitability disorders such as pain and epilepsy. However, physiological mechanisms resulting in M channel potentiation are rare. Here we report that intracellular free zinc directly and reversibly augments activity of recombinant and native M channels. This effect is mechanistically distinct from the known redox-dependent KCNQ channel potentiation. Interestingly, the effect of zinc cannot be attributed to a single histidine- or cysteine-containing zinc binding site within KCNQ channels. Instead, zinc dramatically reduces KCNQ channel dependence on its obligatory physiological activator, phosphatidylinositol 4,5-bisphosphate (PIP_2). We hypothesize that zinc facilitates interactions of the lipid-facing interface of a KCNQ protein with the inner leaflet of the plasma membrane in a way similar to that promoted by PIP_2. Since zinc is increasingly recognized as a ubiquitous intracellular second messenger, this discovery might represent a hitherto unknown native pathway of M channel modulation and provide a fresh strategy for design of M channel activators for therapeutic purposes.

Significance statement

M-type (Kv7, KCNQ) potassium channels are powerful regulators of neuronal and muscular excitability and are validated drug targets for treatment of excitability disorders. The plasma membrane phosphoinositide phosphatidylinositol 4,5-bisphosphate (PIP_2) is required to maintain M channel activity. We report that intracellular free zinc directly and reversibly augments activity of recombinant and native M channels by reducing or virtually abolishing channel requirement for PIP_2, thereby permitting a PIP_2-gated ion channel to operate independently of this important signaling molecule. Given the growing recognition of zinc is as an intracellular second messenger, this phenomenon might represent a hitherto unknown pathway of M channel modulation and provide a fresh strategy for design of M channel-targeting drugs.

\body

M-type (KCNQ, Kv7) K^+ channels are a family of voltage-gated K^+ channels with a very distinctive and robust role in the control of cellular excitability. The channels give rise to non-inactivating K^+ currents with slow kinetics and a very negative activation threshold (-60 mV or even more negative). In combination, these features allow KCNQ channels to remain partially active at voltages near the resting membrane potential of a neuron or a muscle cell and, thus, strongly influence excitability (1, 2). Transient KCNQ channel inhibition leads to reversible increases in neuronal excitability while long-term losses of KCNQ channel activity often result in debilitating excitability disorders (1, 2). Thus, loss-of-function mutations within KCNQ genes underlie some types of epilepsy, deafness and arrhythmias, while transcriptional downregulation in sensory nerves may result in chronic pain (2). Conversely, M channel enhancers ('openers') reduce excitability and are clinically used as antiepileptic drugs (e.g. retigabine) or analgesics (e.g. flupirtine) (3). Therapeutic utility of KCNQ channel openers extends to other disorders linked to deregulated excitability, such as anxiety, stroke, smooth muscle disorders (2, 3); therefore a global quest for specific and selective KCNQ openers is currently underway (3).

The KCNQ channel family contains 5 members (KCNQ1-5, Kv7.1-Kv7.5); KCNQ1 is mostly expressed within the cardiovascular system while other members are predominantly neuronal (1, 2). The most abundant M-type channel within the nervous system is believed to be the heteromeric KCNQ2/3 channel, although other homo-and heteromeric channels are also present (1, 2).

In addition to voltage, KCNQ channels are also sensitive to the plasma membrane phosphoinositide, phosphatidylinositol 4,5-bisphoshpate (PIP_2) (4, 5). Accordingly, G protein coupled receptor-mediated PIP_2 depletion is one of the major mechanisms of excitatory action of endogenous neurotransmitters and neuromodulators such as acetylcholine, angiotensin II, glutamate and others (reviewed in (1, 2)). Excised patch single channel recordings of KCNQ2-4 and KCNQ2/3 channels

revealed that their open probability (P_o) approaches zero when PIP_2 is depleted, whereas increasing concentrations of exogenous PIP_2 raise P_o up to unity (6). It has also been determined that KCNQ3 has over 20 fold higher apparent PIP_2 affinity as compared to KCNQ2 and KCNQ4 (6, 7). As a result, tonic membrane PIP_2 levels in cells such as Chinese hamster ovary (CHO) are sufficient to maintain P_o of KCNQ3 homomers at near unity (at saturating voltages), while homomeric KCNQ2 and KCNQ4 channels display very low P_o values of 0.1 - 0.2 (6, 8). The elucidation of the structural background of the KCNQ channel interaction with PIP_2 is ongoing but several important regions have been identified, including two clusters of positively charged amino acid residues within the channel carboxy-terminus as well as additional clusters within the cytosolic S2-S3 and S4-S5 linkers (reviewed in (9)). All the regions identified thus far are cytosolic and are presumed to facilitate interactions with the negatively charged phosphate groups of PIP_2, facing the cytosol at the inner plasma membrane leaflet. Phosphorylation (10) or methylation (11) of residues within the C-terminal PIP_2 binding site were reported to modulate PIP_2 affinity and, in turn, KCNQ channel activity. Thus, modulation of the KCNQ channel PIP_2 sensitivity may represent a new therapeutic approach to the treatment of excitability disorders, such as epilepsy and pain.

In the present study we report that intracellular zinc ions potently augment the activity of heterologous and native KCNQ channels by reducing channel requirements for PIP_2. The effect of zinc is reversible and most likely direct, as it can be demonstrated in excised membrane patches. Since zinc is being increasingly recognized as an important intracellular second messenger, this effect could represent an alternative regulatory signaling pathway for control over cellular excitability. While intracellular concentrations of free zinc are low (<1 nM; (12)), zinc is accumulated at high levels in various stores, such as ER, mitochondria and synaptic vesicles. In the latter, the concentrations of free zinc could reach millimolar level (13). During synaptic transmission vesicular zinc is released and quantities of zinc translocate to the postsynaptic terminals through zinc permeable channels such as

AMPA receptors (14). Additionally, zinc can be released from cytosolic buffering proteins such as metallothioneins, e.g. in response to acidification (15). Thus, there is clear scope for intracellular zinc signaling in neurons, including, for instance, postsynaptic rises during periods of high activity, hypoxia, neurotrauma etc. Therefore, this acute and rapidly reversible mechanism for 'tuning' KCNQ channel PIP_2 sensitivity by zinc might represent a neuronal feedback mechanism for controlling excitability during periods of hyperexcitability. Yet, since M channel potentiation requires micromolar levels of intracellular zinc, future research is needed to establish if native M channels are indeed subjected to such local concentrations of zinc under physiological or pathophysiological conditions *in vivo*.

Results

Zinc ionophores are KCNQ channel openers. Recent reports (16, 17) identified zinc pyrithione (ZnPy; Fig. S1) as an 'atypical' KCNQ channel opener and suggested that the pyrithione moiety (complexed with zinc) augments KCNQ channel activity by binding to a site within the extracellular pore region (16). It is also well recognized that ZnPy is a zinc ionophore which can effectively deliver free zinc ions across the plasma membrane of living cells (18, 19). Thus, we tested whether the effect of ZnPy on KCNQ channel activity is attributable to the ionophore activity of the former. To this end we overexpressed human KCNQ4 channels in CHO cells and tested the effect of five structurally distinct zinc ionophores on KCNQ4 currents. The following ionophores were used: ZnPy (18) (10 μM), pyrrolidinedithiocarbamate (20) (PDTC; 20 μM), zinc diethyldithiocarbamate (21) (Zn-DEDTC; 30 μM), tetrabutylthiuram disulphide (22) (zinc ionophore I; 20 μM), and 5,7-Diiodo-8-hydroxyquinoline (DIQ; 50 μM) (23). ZnPy and Zn-DEDTC already contained zinc as part of the complex (Fig. S1); other ionophores were used in combination with 25 μM $ZnCl_2$ in the extracellular solution. KCNQ4 has been chosen because among homomeric Kv7 channels it displays the most reproducible and robust

expression in CHO cells (24). Live confocal imaging of intracellular free zinc levels confirmed that all five ionophores produced robust elevations of intracellular zinc (Fig. 1A-F); in each case these elevations were completely reversed by the application of zinc chelator, N, N, N', N', tetrakis (2-pyridylmethyl) etylenediaminepentaethylene (TPEN; 20 μM). TPEN has much higher zinc affinity as compared to other ionophores such as ZnPy and DIQ ($K_d = 10^{-15.6}$ vs. $K_D \approx 10^{-5}$ - 10^{-8} M) (25, 26) and is capable of 'stripping' zinc off intracellular proteins (25) and zinc-sensitive fluorescent indicators (19). We then performed perforated patch voltage clamp recordings to test the effects of these five ionophores on KCNQ4 current amplitude. Strikingly, despite having different chemical structures, all five compounds augmented KCNQ4 amplitude by 2-3 fold (Fig. 1G-L). As with intracellular zinc levels, the effect of each ionophore on KCNQ4 current amplitude was reversed by TPEN. Notably, TPEN did not normally inhibit KCNQ4 current below the baseline but only reversed the ionophore-induced augmentation (Fig. 1L), suggesting that *i)* the effect of TPEN is likely to be mediated by zinc chelation, rather than by a direct effect on the channel; *ii)* tonic cytosolic levels of free zinc in CHO cells are too low to affect channel activity. Similar to KCNQ4, heteromultimeric KCNQ2/3 channels formed by KCNQ2-KCNQ3 concatemers overexpressed in CHO cells were potently augmented by ZnPy, Zn-DEDTC and PDTC; these effects were completely reversed by TPEN (Fig. 2A, B). In accord with previous findings, ZnPy induced leftward shifts of the voltage-dependence of KCNQ4 and KCNQ2/3 from -20.2±1.8 mV to -39.8±1.7 mV (n=8; $p<0.001$) and from -23.2±1.1 mV to -28.6±2.0 mV (n=6; $p=0.089$) respectively (Fig. S2).

Interestingly, Na^+ pyrithione (NaPy; 10 μM) also induced KCNQ4 current augmentation. The effect was slower and smaller in amplitude as compared to that induced by ZnPy, but nevertheless significant (Fig. S3A, B). Thus, NaPy augmented KCNQ4 current by 1.6±0.1 fold (n=7; $p<0.01$) and subsequent transient application of ZnPy to the same cells caused further augmentation (2.1±0.3 fold relative to baseline), which was significantly higher than the NaPy effect ($p<0.01$; Fig. S3A, B).

Finally, application of TPEN (in the presence of NaPy) reverted current amplitude to values that were slightly (but not significantly) below the baseline. Surprisingly, zinc imaging revealed that extracellular application of NaPy produced a moderate but significant elevation of intracellular zinc (Fig. S3C). We measured if our NaPy reagent (purchased from Sigma) is contaminated by zinc using atomic absorption spectroscopy (19) but found that the contamination was negligible. Thus, 100 mM solution of NaPy contained 1.4 ± 0.5 μM zinc (n=4) and in lower dilutions zinc was not reliably detectable. It is therefore likely that the effect was a result of zinc release from intracellular stores or, alternatively, it could be a result of a pyrithione-mediated zinc influx from the extracellular side, since extracellular solutions, while nominally zinc-free, do contain micromolar zinc traces (19). Regardless of the source though, it is clear that *i)* NaPy produces increases in the intracellular free zinc concentration; *ii)* augmentation of KCNQ4 current by NaPy is reversed by the zinc chelator, TPEN. Thus, we conclude that the action of intracellular zinc is responsible for KCNQ4 current augmentation by NaPy.

Intracellular zinc can augment activity of unitary KCNQ channels. Experiments thus far established a correlation between the intracellular zinc levels and macroscopic KCNQ current amplitude. But is intracellular zinc alone sufficient to augment KCNQ channel activity? To answer this question we performed inside-out excised patch recordings of unitary KCNQ2/3 concatemeric channels overexpressed in CHO cells (as described in (6); see Methods). We measured single channel P_o at a saturating voltage (0 mV). Patches with some single-channel activity in cell-attached mode were excised into inside-out configuration; upon excision channel activity declined sharply, displaying almost no activity (Fig. 2C-F), in accord with previous findings (6, 27). This sharp rundown of channel activity upon patch excision is likely due to the depletion of membrane PIP_2 by the membrane-bound lipid phosphatases present in the patch membrane and is characteristic of virtually all PIP_2 sensitive ion channels (28). Addition of increasing concentrations of $ZnCl_2$ to the intracellular side of the patch produced concentration-dependent restoration of KCNQ2/3 channel activity such that their P_o rose

from near zero to 0.26±0.09, 0.68±0.07 and 0.75±0.05 at 10, 50 and 100 μM $ZnCl_2$ respectively (Fig. 2C-F; n=5; $p<0.001$). In our experiments single concatemeric KCNQ2/3 channel current amplitudes at 0 mV were somewhat higher than these reported for channels formed by independently overexpressed KCNQ2 and KCNQ3 subunits (1.21±0.11 pA, n=7 vs. ~0.7 pA (6, 7)), although kinetics and voltage dependence of macroscopic currents were similar (e.g. Fig. S2D). The single-channel experiments demonstrated that intracellular zinc ions are sufficient to augment KCNQ channel activity and, thus, most likely to account for the KCNQ 'opener' action of zinc ionophores. Application of $ZnCl_2$ (up to 50 μM) to the extracellular side of the plasma membrane in whole-cell experiments failed to augment KCNQ4 current but produced weak but rapid inhibitory effect instead (Fig. S4).

Zinc potentiates native M channels in dorsal root ganglion neurons. We next tested if zinc can potentiate the activity of native M channels. M channels are expressed in mammalian somatosensory neurons (especially in 'pain' or nociceptive neurons) and are important for control of their resting excitability (29, 30), ultimately controlling nociceptive signalling (reviewed in (31)). Thus, we tested the effect of intracellular zinc on the M current in cultured small-diameter (presumed nociceptive) rat dorsal root ganglion (DRG) neurons. Similar to the currents produced by overexpressed KCNQ channels, native M current in DRG neurons was also augmented by ZnPy (10 μM) to 1.65±0.24 of basal amplitude (Fig. 3A, B; n=5; $p<0.01$). This effect was completely reversed by 20 μM TPEN, which, however, did not inhibit the current significantly below the basal level. Similarly to CHO cells, ZnPy also produced robust rises in intracellular zinc in cultured neurons (Fig. 3C, D), an effect that was again reversed by TPEN.

To test if intracellular free zinc is sufficient for native M current augmentation we performed whole cell recordings with pipette solution supplemented with 50 μM $ZnCl_2$; in these recordings Ca^{2+}, Mg^{2+} and Ca^{2+} buffers were excluded from the pipette solution. Upon breaking into the whole-cell configuration of patch clamp recording using the control pipette solution there was a small run-up of M

current amplitude (measured as 'tail' current relaxation upon voltage pulse from -30 to -60 mV, see Methods; Fig. 3E). This run-up was significantly potentiated when recording with $ZnCl_2$-containing pipette solution. Accordingly, the plateau M current density was significantly larger in $ZnCl_2$ solution as compared to control (4.8±0.3 pA/pF, n=14 *vs.* *8*.9±1.0 pA/pF, n=14; p≤0.001; Fig. 3F). Thus, native M current in DRG neurons is also potently augmented by intracellular zinc.

Modulation of KCNQ current by zinc is mechanistically distinct from the redox-dependent KCNQ current augmentation. Recently we and others reported augmentation of KCNQ channel activity via the oxidative modification of a triple-cysteine pocket in the channel S2-S3 linker (11, 24, 32). Since zinc can bind to cysteines and form redox-sensitive molecular switches (33), we tested if the effect of zinc on KCNQ channels is also redox-dependent and mediated by the triple-cysteine pocket. We compared the effect of zinc with that of ascorbate, the latter having been shown to augment KCNQ4 channel activity in a redox-dependent way (32). In accord with previous findings, application of 2 mM ascorbate caused 2.5±0.9 fold increase of KCNQ4 current amplitude (n=6; p≤0.01; Fig. 4A, B, G); this effect was reversed by the reducing agent, dithiothreitol (DTT; 2 mM; Fig. 4A, G). In contrast, TPEN (20 μM) did not reverse ascorbate-induced KCNQ4 current augmentation (Fig. 4B, G). Zinc imaging revealed that ascorbate does not produce a measurable increase of intracellular zinc (Fig. S5). On the other hand, the KCNQ4 potentiating effect of ZnPy (and other zinc ionophores) was reversed by TPEN (Fig. 1G-L; Fig. 4D, H) but not DTT (Fig. 4C, H). Most importantly, substitution of three cysteines within the redox-sensitive cysteine pocket by alanines C(156–158)A in KCNQ4 resulted in a channel that was completely insensitive to ascorbate (Fig. 4E, I), yet C(156–158)A mutant channel currents were still sensitive to ZnPy (Fig. 4F, I; 3.1±0.7 fold potentiation, n=5; not different from the wtKCNQ4). These experiments suggest that augmentation of KCNQ currents by zinc is mechanistically distinct from the effect produced by oxidative modification within the reactive cysteine pocket.

In search of the KCNQ zinc binding site. Zinc binding sites in proteins usually contain histidine or cysteine residues (with aspartic or glutamic acids also often participating in zinc coordination) (34). In order to identify a zinc binding site within the KCNQ channels we substituted with alanines all the individual intracellular histidines and also the intracellular cysteines conserved between KCNQ2-4 (Fig. 5A, inset); we used KCNQ4 as a backbone for these experiments. These substitutions included the following residues: histidines at the positions 102, 234, 330, 334, 569 and 669 as well as cysteines at the positions 112, 156-158, 175, 418, 427 and 519. We also tested a KCNQ4 channel with a histidine-less carboxy-terminus - H(330,334,569,669)A as well as a triple-cysteine substitution at positions C(156-158)A (see above). Surprisingly, none of these individual or group His or Cys substitutions abolished channel sensitivity to ZnPy (Fig. 5A). Only in the H569A mutant was the current augmentation somewhat lower (1.6±0.2 fold increase, n=7 vs 2.4±0.4 fold in wtKCNQ4, n=8), but this was not statistically significant. These experiments revealed that neither intracellular histidines nor cysteines (either individually or in clusters) can fully account for zinc-induced KCNQ current potentiation and thus some other mechanisms must be involved.

Surprisingly, H334A displayed dramatically enhanced ZnPy-induced potentiation as compared to wtKCNQ4 (Fig. 5A, Fig. S6); the mutant also had much smaller basal current amplitude (Fig. S6B, D). A similar tendency (although less pronounced) was displayed by the quadruple-His mutant, which also has H334 replaced (Fig. 5A, Fig. S6C, D). Interestingly, H334 in KCNQ4 is equivalent to H328 in KCNQ2, a residue which was identified as one of the key determinants of channel interaction with PIP_2 (5). The reduced apparent affinity to PIP_2 of H334A mutant correlates well with reduced baseline current amplitude. However, the strong enhancement of the baseline current by ZnPy to levels even higher than those produced by wtKCNQ4 may suggest that zinc reduces channel requirements for PIP_2. Our single-channel experiments also hinted to the same hypothesis: KCNQ channels have a permissive requirement for PIP_2 and when membrane PIP_2 is depleted, as in the case of an inside-out excised patch

(28), single KCNQ channels activity runs down rapidly to almost zero (5, 6) (Fig. 2C-F). Yet, addition of zinc to the intracellular side of the plasma membrane was able to rescue the KCNQ channel activity without replenishment of PIP_2. We therefore asked if zinc can indeed interfere with channel requirement for PIP_2.

Zinc reduces KCNQ channel PIP_2-dependence. First, we tested the effect of intracellular zinc on KCNQ3, a channel that, in contrast to KCNQ2 and KCNQ4, has high PIP_2 affinity (6), such that tonic PIP_2 levels in CHO cells are sufficient to maintain tonic maximal P_o of this channel near unity (6). Since the KCNQ3 channel expresses poorly as a homomer (35, 36), we used KCNQ3 with a pore domain mutation A315T ($KCNQ3^T$), which strongly increases KCNQ3 current amplitude without changing apparent PIP_2 affinity (7, 36, 37). Interestingly, neither ZnPy nor PDTC had any effect on the $KCNQ3^T$ current amplitude (Fig. 5B, E, D, G), suggesting that the effects of PIP_2 and zinc on channel activity are non-additive, meaning that zinc would have little effect on a given KCNQ subunit under conditions when the level of PIP_2 is saturating.

We then disabled two known C-terminal PIP_2 interacting sites in $KCNQ3^T$ by *i)* deleting a linker between helices A and B (positons 411-508) that harbors a cluster of basic residues (including K425, K432, and R434) (38) and *ii)* introducing mutations R364A and H367C that neutralized the PIP_2 interacting site at the junction between the S6 and C-terminal helix A (5, 39); we labelled this mutant '$KCNQ3^T$-ΔPIP_2-C_{term}'. Charge-neutralizing mutations within either of these sites were shown to reduce channel PIP_2 affinity (5, 38, 39). Accordingly, $KCNQ3^T$-ΔPIP_2-C_{term} current amplitude was reduced over 10 fold as compared to the $KCNQ3^T$ channel (103.25±28.34 pA, n=12 vs. 1170±370 pA, n=10, $p \leq 0.001$). Strikingly, both ZnPy and PDTC produced 5-7 fold augmentation of $KCNQ3^T$-ΔPIP_2-C_{term} current amplitude (Fig. 5C, D, F, G). These data suggest that the increased PIP_2 dependence of the $KCNQ3^T$-ΔPIP_2-C_{term} mutant can be compensated by intracellular zinc.

Next, we used a similar strategy to reduce PIP_2 affinity of KCNQ4 to test how this would affect zinc effects on this channel. This time we targeted a different PIP_2-interacting site, the S4-S5 linker. We neutralized one of the basic residues by introducing a K236L substitution (Fig. 5A, inset) at a position equivalent to K222 in KCNQ3, which was shown to be involved in the interaction with PIP_2 (17). As in the case with $KCNQ3^T$-ΔPIP_2-C_{term}, KCNQ4 K236L mutant had much reduced current amplitude as compared with the wtKCNQ4 (Fig S7, A-D). However, ZnPy produced much stronger current augmentation of the mutant: 16.1±4.4 fold (n=10) *vs.* 2.4±0.4 fold (n=7; $p \leq 0.01$; Fig. S7A, B, E). To probe further the relationships between the channel PIP_2 requirement, PIP_2 levels and potentiation by zinc, we increased tonic PIP_2 levels in CHO cells by overexpressing the key enzyme of PIP_2 synthesis, PI(4)5-kinase (which phosphorylates phosphatidylinositol 4-phosphate to PIP_2); this maneuver has been shown to increase maximal P_o and macroscopic current density of KCNQ2 and KCNQ2/3 in CHO cells (6). PI(4)5-kinase overexpression indeed significantly increased current amplitudes of both wtKCNQ4 and KCNQ4 K236L, and, as expected, had a stronger effect on the latter (Fig. S7C, D). In PI(4)5-kinase overexpressing CHO cells ZnPy still augmented current amplitudes of both wt and K236L mutant channels but, notably, the maximal current amplitudes in the presence of ZnPy were the same in CHO cells with and without PI(4)5-kinase overexpression (Fig. S7C, D). Accordingly, the degree of the ZnPy-induced augmentation of the KCNQ4 K236L current (relative to baseline) in the presence PI(4)5-kinase was strongly reduced (Fig. S7E) and was no longer different from the augmentation of wtKCNQ4 in the absence of PI(4)5-kinase.

Collectively, experiments presented in Fig. 5B-G and Fig. S7, together with the single-channel data (Fig. 2C-F), suggest that *i)* at saturating PIP_2 levels intracellular zinc can no longer increase channel activity; *ii)* the lower the level of channel saturation with PIP_2, the higher is the augmenting effect of zinc; *iii)* even when PIP_2 saturation is below the threshold for channel activation (e.g. in inside-out patches), KCNQ channels can still be activated by zinc.

Finally, we asked how presence of intracellular zinc affects KCNQ channel sensitivity to acute PIP_2 depletion and recovery. We utilized the voltage sensitive phosphatase from *Ciona intestinalis* (ciVSP). This enzyme is activated by strong depolarization; when overexpressed it is capable to robustly deplete membrane PIP_2 (40) and almost completely inhibit KCNQ channel activity (41, 42). We overexpressed ciVSP with either KCNQ4 or with KCNQ2/3 concatemer in CHO cells and recorded currents during the ciVSP activation. Cells were held at -80 mV and three-step pulses (Fig. $6A_1$) were applied: *i)* 1-s step to -20 mV (close to the threshold for ciVSP activation (40, 43) but near the half-maximal voltage for KCNQ channel activation (2)); *ii)* 1-s step from -20 mV to 120 mV (close to the saturating voltage for ciVSP (40, 43)); *iii)* 30-s step from 110 mV to -20 mV. At the end of the protocol voltage was returned to the holding potential. In the control conditions during step *i)* KCNQ channels are activated; during step *ii)* KCNQ channel current is first increased due to the increased driving force but then begin to decline due to the ciVSP activation and PIP_2 depletion. At the beginning of step *iii)* PIP_2 is depleted and KCNQ channels are inhibited but because of the ciVSP deactivation and PIP_2 re-synthesis, at the end of this step KCNQ activity recovers (Fig. $6A_1$, B_1, C_1, D_1; black traces). Since steps *i)* and *iii)* are recorded at the same voltage (-20 mV), the difference between current amplitudes at the end of step *i)* and the beginning of step *iii)* represents KCNQ current inhibition by the ciVSP-induced PIP_2 depletion, while the difference between amplitudes at the end of step *i)* and the end of step *iii)* represents current recovery due to PIP_2 re-synthesis (41). In accord with previous findings, ciVSP activation induced 70-80% inhibition of both KCNQ2/3 (Fig. 6A, B) and KCNQ4 (Fig. 6C, D) and in both cases current completely recovered at the end of the step *iii)*. Application of either ZnPy or PDTC completely abolished PIP_2-dependent inhibition of both KCNQ channels (Fig. $6A_1$, B_1, C_1, D_1; red traces). Application of TPEN after (and in the presence of) ZnPy, recovered the ability of ciVSP to inhibit KCNQ2/3 channel (Fig. $6A_1$, A_2).

In order to test if zinc inhibits ciVSP itself, we used an optical method of measuring ciVSP activity in which we co-expressed the enzyme in CHO cells together with KCNQ4 and the optical PIP_2 reporter PLC-δPH-GFP (44) and measured its translocation from membrane to cytosol in response to depolarization by extracellular solution containing 150 mM KCl instead of NaCl (45). Intracellular K^+ concentration in CHO cells is ~140 mM (46), thus such maneuver depolarized membrane potential to ~+2 mV, which is sufficient to trigger measurable ciVSP activation (43, 45). Accordingly, confocal imaging of the plasma membrane PIP_2 labelled by PLC-δPH-GFP revealed clear and reversible, depolarization-induced PIP_2 depletion manifested in PLC-δPH-GFP translocation and an increase in cytosolic fluorescence (and concomitant decrease in membrane fluorescence; Fig. 6E). This translocation was not affected by extracellular application of ZnPy, suggesting that zinc does not significantly affect ciVSP activity.

Muscarinic inhibition of KCNQ channels is mediated by $G_{q/11}$-induced activation of phospholipase C (PLC) via depletion of PIP_2 (4, 5). Additionally, inositol trisphosphate-dependent Ca^{2+} transients (mediated by calmodulin) and diacylglycerol-dependent protein kinase C (PKC) phosphorylation are also thought to contribute to muscarinic KCNQ channel inhibition. Both of these additional mechanisms are thought to work by decreasing channel PIP_2 affinity (reviewed in (2)). Thus, if intracellular zinc reduces channel dependence on PIP_2, it would be expected that in the presence of zinc muscarinic inhibition of KCNQ channels will be reduced or abolished. Indeed, in CHO cells overexpressing KCNQ4 and M1 muscarinic receptor pre-application of ZnPy reduced KCNQ current inhibition by M1-specific agonist oxotremorine-M (Oxo-M) from 69±9% (n=7) to 9±3% (n=7; $p<0.01$; Fig. S8).

Discussion.

The major findings of this study are the following. *i)* Intracellular zinc strongly potentiates native and recombinant KCNQ channel activity. *ii)* Any zinc ionophore is a potential KCNQ channel opener. *iii)* Zinc reversibly reduces or perhaps even abolishes KCNQ channel requirement for PIP_2. *iv)* Mechanistically, the zinc effect is distinct from the known redox-dependent KCNQ channel potentiation; also, the effect cannot be attributed to a histidine- or cysteine-containing binding site.

Several lines of evidence indicate that zinc strongly reduces KCNQ channel requirement for PIP_2. Thus, *i)* unitary KCNQ2/3 channel activity quickly runs down upon patch excision, due to PIP_2 depletion (5, 28); yet, addition of free zinc to the intracellular side of the membrane maximizes channel activity (Fig. 2C-F). *ii)* KCNQ3 is insensitive to zinc ionophores (Fig. 5B-G; (17)); this channel has highest apparent affinity for PIP_2 in the KCNQ family and its tonic P_o max at saturating voltages is close to unity, presumably due to saturation with PIP_2 (6). Removal of C-terminal PIP_2 interacting residues resulted in a channel with much lower tonic activity which can be 'rescued' by intracellular zinc (Fig. 5B-G). *iii)* Similarly, efficacy of ZnPy to augment KCNQ4 current is higher for the mutant with reduced PIP_2 affinity. *iv)* Elevation of tonic PIP_2 levels by overexpression of PI(4)5-kinase reduced KCNQ channel sensitivity to zinc. *v)* Finally, acute PIP_2 depletion by ciVSP or M1 receptor activation sharply inhibits KCNQ2/3 and KCNQ4 currents but this inhibition is abolished by zinc (Fig. 6A-D, Fig. S8). It appears that zinc can compensate for the channel's desaturation with PIP_2 due to either acute PIP_2 depletion or reduction in PIP_2 affinity. On the other hand, the more saturated a channel protein is with PIP_2, the lower is zinc efficacy.

How might zinc interact with KCNQ channels and so dramatically affect channel-PIP_2 interaction; is there a unique zinc binding site? It is worth noting that interaction between KCNQ channels and PIP_2 cannot be pin-pointed to a unique, localized binding site. Instead, the channel appears to form a broad PIP_2-interacting interface whereby basic residues, spread along all main

cytosolic domains of a channel, participate in electrostatic interactions with the negatively charged headgroup phosphates of PIP_2. Thus, basic residues in the S2-S3 linker (47, 48), S4-S5 linker (17, 49), S6-proximal C-terminus linker (5, 39), C-terminal A-B helix linker (38) and distal C-terminus (49) were identified and charge neutralisation mutations within most of these sites resulted in reduced apparent PIP_2 affinity and reduced tonic channel activity (reviewed in (9)). Another important point is that not only PIP_2, but other phosphoinositides such as PIP, PI(3,4)P, PI(3,4,5)P (6, 27) and even other phospholipids such as lysophosphatidic acid and sphingosine-1-phosphate (27) can activate KCNQ channels. Under normal physiological circumstances these interactions are thought not to affect KCNQ channel activity significantly due to the low plasma membrane abundance of these other lipids (relative to that of PIP_2) (2, 27). However, should the affinity of channel-lipid interaction increase, these minor phospholipids may move into play. One explanation for the activating effect of zinc could therefore be that it serves as electrostatic 'glue' that stabilizes interaction of the KCNQ channel's phospholipid interface with inner leaflet of the plasma membrane (Fig. 7). Perhaps by interacting with the negatively-charged amino-acid residues within the channel-membrane interface zinc ions strengthen the interactions of the positively-charged amino-acids with negatively-charged headgroups of phospholipids. This may either reduce the channel's selectivity towards phospholipids (such that other negatively charged lipids may become capable to substitute for PIP_2 anchoring) or dramatically increase its apparent affinity for PIP_2, or have a combination of the above effects resulting in stabilizing channel opening.

Interestingly, magnesium has been shown to decrease KCNQ channel activity, presumably by shielding PIP_2 and weakening KCNQ channel-PIP_2 interaction (50). It is unclear why the effects of zinc and magnesium on KCNQ channel activity are so different, one consideration though is that as a transition metal, zinc has a much higher (as compared to magnesium) ability to form chelate complexes (see e.g. http://www.coldcure.com/html/stability_constants.html) and, potentially, to coordinate tertiary

protein structures. Thus, zinc could potentially be better suited to stabilize KCNQ channel-membrane interactions. Yet, future structural studies are required to comprehensively address this question.

Another intriguing question is whether the 'PIP_2 rescue' effect of zinc can affect other PIP_2-sensitive channels. We tested the effect of ZnPy on another PIP_2-sesnitive channel, Kir2.3 (51) as well as on a PIP_2-insensitive channel, Kv1.4 (42). However, both of these channels were inhibited by ZnPy to a various degree (Fig. S9). The likely explanation here is that zinc might act as a pore blocker or inhibitor of these channels; there could also be additional inhibitory mechanisms (e.g. induced by the ionophore). Thus, while zinc may indeed reduce PIP_2 dependence of other PIP_2-sensitive channels, only those reasonably insensitive to zinc as a blocker would exhibit augmentation of activity. KCNQ channels are indeed not very sensitive to such inhibition (Fig. S4).

Our hypothesis (Fig. 7) can also explain highly variable efficacies of ZnPy observed in various studies. Thus, a dramatic 24-fold augmentation of KCNQ4 current (at saturating voltages) was reported (16), whereas the effect on KCNQ2/3 channels in that study was much smaller (~2-fold). In our hands the augmentation of KCNQ4, KCNQ2/3 and native M channels by ZnPy, other zinc ionophores and by intracellular zinc in whole-cell recordings was in the range of 1.5 – 3 fold (Fig. 1-3, (52)). However, much stronger effects were observed when either PIP_2 levels were depleted (Fig. 2C-F) or when PIP_2 affinity of the channels was reduced by mutagenesis (Fig. 5; Fig. S6). Thus, it is expected that the efficacy of ZnPy to augment KCNQ channel activity in any particular experimental setting will strongly depend on the channel saturation with PIP_2.

Our findings confirm the discovery of ZnPy as a potent KCNQ channel opener (16), however, our study differs significantly from the original publication in the interpretation of the mechanism of ZnPy action. It was originally proposed that the effect is produced by the pyrithione moiety (in complex with zinc) binding to the channel's pore region from the extracellular side (16). Below we briefly discuss differences between the study (16) and our investigation. *i)* Xiong and colleagues

reported only marginal effects of other zinc ionophores, DEDTC, DIQ and α-tocopherol on KCNQ2 channels. Zinc ionophore activity of α-tocopherol is not well documented, but the lack of effect of DEDTC and DIQ is perplexing as in our hands both ionophores (as well as three others) strongly augmented KCNQ currents (Fig. 1). We also show that all the ionophores tested produced strong intracellular zinc accumulation (Fig. 1); since no such measurements were performed in study (16), we suggest that under their experimental conditions ZnPy was superior to other ionophores in loading cells with zinc. *ii)* Dialysis of 10 μM ZnPy through the recording pipette did not significantly affect KCNQ2 current amplitude but extracellular ZnPy was still effective. It was therefore suggested that ZnPy acts from the extracellular side. However, this experiment is hard to interpret as it is not clear how much *free* intracellular zinc has been delivered in such a way. Our experiments demonstrated that direct application of $ZnCl_2$ to the intracellular side of the excised patch (Fig. 2C-F) or by the dialysis through the whole cell pipette (Fig. 3F) strongly potentiated both recombinant and native KCNQ channels. *iii)* The effect of 20 μM NaPy on KCNQ2 current was marginal; it was proposed that KCNQ2 interacts with pyrithione with low affinity, but the affinity is increased when pyrithione is in complex with zinc (16). In our experiments NaPy produced a significant increase of KCNQ4 current but, importantly, also elevated intracellular zinc, although both effects were much less pronounced as compared with ZnPy. This difference may arise from lower intracellular zinc store load of cells used in the previous study.

Zinc is increasingly recognized as ubiquitous second messenger, perhaps comparable in this regard to calcium (53). Cytosolic free zinc levels at rest are too low to affect KCNQ channel activity (<1 nM; (12)); this is a likely explanation for the fact that while TPEN reversed KCNQ current augmentation by exogenous zinc, it rarely reduced the amplitude of KCNQ channels overexpressed in non-excitable CHO cells below the baseline. Yet, in the synaptic vesicles of neurons zinc can reach millimolar levels (13); another releasable pool of zinc is bound to intracellular proteins such as metallothioneins (15). Vesicular zinc is released during synaptic transmission and loads postsynaptic

terminals through zinc permeable channels (e.g. AMPA (14)). Zinc can also be released from cytosolic buffers in response to acidification (15) observed in hypoxic conditions. In a recent study FluoZin3 zinc imaging revealed large intracellular zinc transients (comparable to rises recorded in this study in response to zinc ionophores) in hippocampal pyramidal neurons in response to oxidative stress (14). It is therefore conceivable that augmentation of KCNQ channel activity by postsynaptic zinc accumulation could constitute a strategy to survive excitotoxicity produced by ischemia or other conditions linked to over-excitability, such as epileptic seizures. A strong protective role of M channels in ischemic brain injury and stroke has been demonstrated (8, 9). Importantly, since zinc makes KCNQ channels virtually insensitive to $G_{q/11}$ receptor inhibition, postsynaptic zinc elevations could maintain M channel activity in the face of enhanced neurotransmitter release. Further research is required to test these intriguing hypotheses.

Methods

Cell culture, transfection, mutagenesis. HEK 293 cells were cultured in DMEM and CHO cells in DMEM:F12 (1:1) media, both supplemented with GlutaMax I, 10% fetal calf serum, penicillin (50 U/ml), and streptomycin (100 μg/ml). DRG neurons from 7 days old Wistar were dissociated as previously described (29) and cultured in DMEM supplemented as above on glass coverslips that were coated with poly-d-lysine and laminin for 2–5 days in a humidified incubator (37^{o}C, 5% CO2). CHO or HEK293 cells were transfected using Fugene® HD (Promega) with the following cDNA (routinely subcloned into pcDNA3.1): human KCNQ4 (accession number AF105202) and its mutants; KCNQ2/3 concatemer (kind gift from Snezana Maljevic, Tubingen University, Germany); KCNQ3 A315T and its mutants (kindly provided by Mark Shapiro, University of Texas Health Science Center at San Antonio, Texas, USA); Type 1a PI(4)5-kinase (54); PLC-δPH-GFP (55); ciVSP (40) (kind gift from Tibor Rohacs, Rutgers University, New Jersey, USA). The point mutations and truncations were introduced by site-directed mutagenesis using standard techniques and verified by sequencing.

Whole-cell and perforated patch recordings. All recordings were made using an EPC10 amplifier in combination with PatchMaster v2 software and analyzed using the FitMaster v2 (all from HEKA Instruments). Most of the whole-cell recordings were made using perforated patch clamp technique. The standard bath solution contained the following (in mM): 160 NaCl, 2.5 KCl, 1 $MgCl_2$, 2 $CaCl_2$, 10 HEPES, pH 7.4 (with NaOH), 305–310 mosm/kg. The standard pipette solution contained the following (in mM): 160 KCl, 5.0 $MgCl_2$, 5.0 HEPES, 0.1 BAPTA, 3 K_2ATP, NaGTP, pH7.4 (with KOH), supplemented with amphotericin B (200-400 μg/ml). The access resistance was typically within 5 MΩ. When recording from DRG neurons, small-diameter cells (~20 μm) were selected. When applying $ZnCl_2$ (50 μM) to DRG neuron's cytosol via patch pipette dialysis the conventional whole-cell configuration was used. The pipette solution contained the following (in mM): 120 K-acetate, 35 KCl, 5 NaCl, 3NaATP, 0.1 GTP, 10 HEPES, pH 7.3 with KOH. KCNQ/M currents were measured by

1-s square voltage pulse to -60 mv from a holding potential of 0 mV (CHO cells) or -30 mV (DRG neurons) applied every 2-s. Recombinant KCNQ current amplitude was defined as XE991-sensitive steady-state outward current amplitude at 0 mV. Native M current amplitude was defined as XE991-sensitive 'tail' current amplitude upon voltage step from -30 to -60 mV. In experiments with ciVSP, cells were held at -80 mV and 3-step voltage pulses (1-s steps to -20 mV followed by 1-s step to 120 mV and a 30-s step back to -20 mV) were applied with 3-s intervals.

Single-channel recording. The inside-out KCNQ current recording and analysis were performed as before (6, 8). Channel activity was recorded 48–72 h after transfection; pipettes had resistances of 7–15 MΩ when filled with a solution of the following composition (in mM): 150 NaCl, 5 KCl, 1 $MgCl_2$, and 10 HEPES, pH 7.4 (with NaOH). Extracellular solution contained the following (in mM): 175 KCl, 4 $MgCl_2$, and 10 HEPES, pH 7.4 (with KOH). The resting membrane voltage was assumed to be 0 mV. Currents were recorded using an EPC 10 amplifier (HEKA Instruments), sampled at 5 kHz, and filtered at 0.5–1 kHz. Single-channel data (including P_o histogram generation) were analyzed using FitMaster software (HEKA Instruments). Methods for event analysis, P_o and single-channel amplitude calculation were as in (6).

Fluorescence imaging. Intracellular zinc imaging was performed as in (19). CHO cells or DRG cultures were loaded with FluoZin-3AM (5 μM for 30 min at 37^{o}C in the presence of 0.02% pluronic F-127). Cells were washed with extracellular bath solution composed of the following (in mM): 160 NaCl; 2.5 KCl; 2 $CaCl_2$; 1 $MgCl_2$; and 10 HEPES; pH 7.4 (with NaOH). Cells were imaged using a Leica SP5 fluorescence imaging system assembled on a Leica DMI6000 microscope and illuminated with 488 nm light for 1200 ms (400 Hz) with a 2 s interval. In confocal PIP_2 imaging experiments HEK293 cells transfected with PLC-δPH-GFP and KCNQ4 were illuminated using Nikon A1 confocal microscope with a 488 nm argon laser. Images were collected on an electron multiplying CCD camera (DQC-FS; Nikon) using NIS Elements 4.0 imaging software (Nikon), which was also used for analysis.

Statistics. All data are given as mean±S.E.M. Differences between groups were assessed by Student's t test (paired or unpaired, as appropriate) or one-way ANOVA with Bonferroni correction. The differences were considered significant at $p \leq 0.05$.

Acknowledgments. We thank Ewa Jaworska and Hongchao Men for technical assistance, Dr. Crystal Archer for help with the PIP_2 binding site neutralization and Dr Alexandre Vakurov for valuable advice on zinc chemistry. This work was supported by the MRC (grant MR/K021303/1 to C.P. and N.G.), National Natural Science Foundation of China (grant 81201642 to H.G.) and Hebei Province Department of Education to (grant BJ2017004 to DY).

Figure legends.

Figure 1. Zinc ionophores potentiate KCNQ4. (A-E), Fluorescence imaging of CHO cells loaded with zinc fluorophore, FluoZin^{TM}-3AM. Example time course of changes in FluoZin-3 fluorescence during application of (**A**) zinc pyrithione (ZnPy;10 μM), (**B**) pyrrolidinedithiocarbamate (PDTC; 20 μM), (**C**) zinc diethyldithiocarbamate (Zn-DEDTC; 30 μM), (**D**) tetrabutylthiuram disulfide (zinc ionophore I; 20 μM), (**E**) 5,7-Diiodo-8-hydroxyquinoline (DIQ; 50 μM). PDTC, DIQ and zinc ionophore I were supplemented 25 μM $ZnCl_2$. At the end of each recording zinc chelator, N, N, N', N', tetrakis (2-pyridylmethyl) etylenediaminepentaethylene (TPEN; 20 μM) was added (still in the presence of appropriate ionophore). In these and all other time-course plots, periods of drug applications are indicated with the grey shading. (**F**) Summary of the experiments presented in (**A-E**); number of cells is indicated within the bars; asterisks indicate significant difference from the basal fluorescence with ***$p<0.001$ (paired t-test). (**G-K**) Perforated patch clamp recordings from the KCNQ4-transfected CHO cells showing the time courses for effects of zinc ionophores and TPEN (as labelled; applied as in panels **A-E**) on the KCNQ4 current amplitude. At the end of each recording a specific KCNQ channel inhibitor, XE991 (10 μM), was applied. Example current traces are shown on the right; voltage protocol is given in the top inset in (**G**). (**L**) Summary of the experiments presented in (**G-K**); number of cells is indicated within the bars; asterisks indicate significant difference from the basal fluorescence with **$p<0.01$ (paired t-test).

Figure 2. Effect of intracellular zinc on KCNQ2/3 channels. (**A**) Perforated patch clamp recordings from the CHO cells transfected with the KCNQ2/3 concatemer showing the effects of DEDTC (30 μM), TPEN (20 μM) and XE991 (10 μM) (as labelled) on the M current amplitude. Example current traces are shown on the right. (**B**) Summary of the effects of ZnPy, PDTC and DEDTC on KCNQ2/3 currents; recordings were made as in Fig. 1**G-K** and Fig. 2 (**A**). Number of cells is indicated within the bars; asterisks indicate significant difference from the baseline with **$p<0.01$

(paired t-test). (**C**) Current records from a patch of CHO cell membrane containing a single KCNQ2/3 channel in cell-attached mode with various concentrations of $ZnCl_2$ in the 'cytosolic' bath solution. (**D**), Each 10 s sweep during the experiment was analyzed for channel open probability (P_o), and the time course of the P_o during the experiment is plotted. (**E**) All-point amplitude histograms for the sweeps shown on the panel (**C**). (**F**) Summary of the effect of intracellular $ZnCl_2$ (10-100 μM) on the KCNQ2/3 channel open probability (P_o). Number of recordings is indicated within the bars; asterisks indicate significant difference from the control with **p<0.01 (paired t-test).

Figure 3. Effect of intracellular zinc on the endogenous M current in dorsal root ganglion (DRG) neurons. (**A**) Time course of the effect of ZnPy (10 μM), TPEN (20 μM) and XE991 (3 μM) on the M-like K^+ current recorded from the small-diameter cultured rat DRG neuron. Example current traces are shown on the right; voltage protocol is depicted below the traces; summary is given in (**B**). (**C**) Fluorescence imaging of DRG cultures loaded with zinc fluorophore, FluoZin™-3AM. Shown is the example time course of changes in FluoZin-3 fluorescence during application of ZnPy (10 μM) and TPEN (20 μM). Example fluorescence micrographs are shown in the inset on the right; summary is given in (**D**). Number of recordings is indicated within the bars; asterisks indicate significant difference from the baseline with *p<0.05 or **p<0.01 (paired t-test). (**E**) Example time courses of changes in M-like current amplitude in DRG neurons upon breaking into whole-cell configuration with pipette solution containing no added zinc, Ca^{2+} or divalent cation buffers (Control) or the same solution supplemented with 50 μM $ZnCl_2$; summary is given in (**E**). In bar charts number of recordings is indicated within the bars. Asterisks indicate significant difference from the control with *p<0.05, **p<0.01 or ***p<0.001 (paired or unpaired t-test).

Figure 4. Mechanism of KCNQ channel potentiation by zinc is distinct form the redox-dependent modulation. (**A, B**) Perforated patch clamp recordings from the KCNQ4-transfected CHO cells; KCNQ4 current augmentation by ascorbate (Asc., 2 mM) was reversed by the reducing agent

dithiothreitol (DTT, 2 mM) (**A**) but not by 20 μM TPEN (**B**). Example current traces are shown in the insets. (**C, D**) Experiments and analysis similar to these shown in (**A-C**) but ZnPy (10 μM) was applied instead of ascorbate. In this case the KCNQ4 augmentation was reversed by TPEN but not DTT. (**E, F**) Effect of ascorbate (**E**) but not ZnPy (**F**) is abolished in KCNQ4 channel with C-to-A substitutions at the positions 156, 157 and 158. (**G**), (**H**) and (**I**) summarize the ascorbate (**G**) and ZnPy (**H**) experiments on wtKCNQ4 and the experiments on the KCNQ4 C(156-158)A. Number of recordings is indicated within the bars. Asterisks in (**G**), (**H**) denote significant difference from the group indicated by the line connector with *p<0.05 or **p<0.01 (paired t-test). Symbols in (**I**) indicate significant difference from either control (**p<0.001; paired t-test) or from current amplitude in the presence of ZnPy (#p<0.05; paired t-test).

Figure 5. Intracellular zinc affects KCNQ channel interaction with PIP_2. (**A**) Summary of the ZnPy-induced current augmentation (normalized to baseline) for single C-to-A and H-to-A KCNQ4 mutants as well as for the C(156-158)A triple mutant and H(330,334,569,669)A quadruple mutant expressed in CHO cells. Schematic depiction of substitutions is shown in the inset. Asterisks indicate significant difference from wtKCNQ4 (***p<0.001; one-way ANOVA with Bonferroni correction). (**B-G**) Comparison of the effects of 10 μM ZnPy (**c-e**) and 20 μM PDTC (**f-h**) on the amplitude of the KCNQ3 A315T ($KCNQ3^T$; **B, E**) or $KCNQ3^T$ with the C-terminal PIP_2-interacting sites neutralized: deletion of A-B linker (positons 411-508) and R364A and H367C substitutions ($KCNQ3^T$-ΔPIP_2-C_{term}; **C, F**). (**D**) and (**G**) summarize the effects. Number of experiments is indicated within the bars. Asterisks indicate significant difference from control (**p<0.001; paired t-test).

Figure 6. Intracellular zinc abolishes KCNQ channel inhibition by the voltage-sensitive phosphatase ciVSP. (**A-B**) Effects of 10 μM ZnPy (**A**) and 20 μM PDTC (**B**) on the ciVSP-induced inhibition of KCNQ2/3 concatemers in CHO cells. Example current traces are shown in ($\mathbf{A_1}$) and ($\mathbf{B_1}$); voltage protocol is given in the inset above traces in ($\mathbf{A_1}$). ($\mathbf{A_2}$) shows a time course of the effects of

ZnPy and recovery by TPEN on the ciVSP-induced inhibition of KCNQ2/3 (same experiment as that shown in **A_1**). (**A_3**) and (**B_2**) summarize the effect of zinc ionophores on the ciVSP-induced KCNQ2/3 current inhibition. (**A_4**) and (**B_3**) summarize the recovery from the ciVSP-induced inhibition in either the control conditions or in the presence of the ionophore (as indicated). Number of experiments is indicated within the bars. Asterisks and number symbols indicate significant difference from control and ZnPy, respectively ($p<0.001$; paired t-test). (**C-D**) are similar to (**A-B**) but KCNQ4 was tested. (**E**) Shows confocal imaging of the effect of ciVSP activation by depolarization (150 mM extracellular KCl; with or without 10 μM ZnPy, as indicated) on the membrane localization of the optical PIP_2 reporter PLC-δPH-GFP. Example time course is shown in (**E_1**), images taken at the times indicated by the letters in (**E_1**) are shown in (**E_2**); corresponding intensity line-scans (at a position indicated by dotted red line in E_2a) are shown below the images. Summary of the changes in cytosolic fluorescence intensity is shown in (**E_3**); number of experiments is indicated within the bars. Asterisks indicate significant difference from control ($p<0.001$; repeated measures ANOVA).

Figure 7. Hypothesis for the KCNQ channel stabilization by the PIP_2 and intracellular zinc. Panel (**A**) shows an active channel in the presence of saturating PIP_2 concentration; (**B**) shows a channel inhibited by PIP_2 depletion (e.g. due to PLC or ciVSP activation). Sown in (**C**) is a channel in the absence of membrane PIP_2 but stabilized by zinc, e.g. via 'shielding' the negatively-charged residues and coordinating the channel-membrane interface to strengthen the interactions with other phospholipids. Shown in (**D**) is a scenario of a sub-saturating membrane PIP_2 level when the channel activity is maximized by zinc due to increased stability of interaction with PIP_2 and other membrane phospholipids.

References

1. Delmas P & Brown DA (2005) Pathways modulating neural KCNQ/M (Kv7) potassium channels. *Nat Rev Neurosci* 6:850-862.
2. Gamper N, Shapiro, M.S. (2015) KCNQ Channels. *Handbook of Ion Channels*, ed Zheng J, Trudeau, M.C. (CRC Press, Boca Raton, FL), 1st Ed, pp 275-306.
3. Gribkoff VK (2008) The therapeutic potential of neuronal Kv7 (KCNQ) channel modulators: an update. *Expert Opin Ther Targets* 12(5):565-581.
4. Suh B & Hille B (2002) Recovery from muscarinic modulation of M current channels requires phosphatidylinositol 4,5-bisphosphate synthesis. *Neuron* 35(3):507-520.
5. Zhang H*, et al.* (2003) PIP_2 activates KCNQ channels, and its hydrolysis underlies receptor-mediated inhibition of M currents. *Neuron* 37(6):963-975.
6. Li Y, Gamper N, Hilgemann DW, & Shapiro MS (2005) Regulation of Kv7 (KCNQ) K^+ channel open probability by phosphatidylinositol (4,5)-bisphosphate. *J Neurosci* 25(43):9825-9835.
7. Telezhkin V, Brown DA, & Gibb AJ (2012) Distinct subunit contributions to the activation of M-type potassium channels by $PI(4,5)P_2$. *J Gen Physiol* 140(1):41-53.
8. Li Y, Gamper N, & Shapiro MS (2004) Single-channel analysis of KCNQ K^+ channels reveals the mechanism of augmentation by a cysteine-modifying reagent. *J Neurosci* 24(22):5079-5090.
9. Zaydman MA & Cui J (2014) PIP_2 regulation of KCNQ channels: biophysical and molecular mechanisms for lipid modulation of voltage-dependent gating. *Frontiers Physiol* 5:195.
10. Salzer I*, et al.* (2016) Phosphorylation regulates the sensitivity of voltage-gated Kv7.2 channels towards phosphatidylinositol-4,5-bisphosphate. *J Physiol*. 595(3):759-776.

11. Kim HJ, *et al.* (2016) Protein arginine methylation facilitates KCNQ channel-PIP_2 interaction leading to seizure suppression. *eLife* 5 pii: e17159.

12. Takeda A (2014) Zinc signal in brain functions. *Zinc signals in cellular functions and disorders*, ed Fukada T, Kambe, T. (Springer Japan), pp 161-181.

13. Sindreu C & Storm DR (2011) Modulation of neuronal signal transduction and memory formation by synaptic zinc. *Fron Behav Neurosci* 5:68.

14. Medvedeva YV, Ji SG, Yin HZ, & Weiss JH (2017) Differential Vulnerability of CA1 versus CA3 Pyramidal Neurons After Ischemia: Possible Relationship to Sources of Zn^{2+} Accumulation and Its Entry into and Prolonged Effects on Mitochondria. *J Neurosci* 37(3):726-737.

15. Kiedrowski L (2014) Proton-dependent zinc release from intracellular ligands. *J Neurochem* 130(1):87-96.

16. Xiong Q, Sun H, & Li M (2007) Zinc pyrithione-mediated activation of voltage-gated KCNQ potassium channels rescues epileptogenic mutants. *Nat Chem Biol* 3(5):287-296.

17. Zhou P, *et al.* (2013) Phosphatidylinositol 4,5-bisphosphate alters pharmacological selectivity for epilepsy-causing KCNQ potassium channels. *Proc Natl Acad Sci U S A* 110(21):8726-8731.

18. Magda D, *et al.* (2008) Synthesis and anticancer properties of water-soluble zinc ionophores. *Cancer research* 68(13):5318-5325.

19. Huang D, *et al.* (2016) Redox-Dependent Modulation of T-Type Ca^{2+} Channels in Sensory Neurons Contributes to Acute Anti-Nociceptive Effect of Substance P. *Antioxid Redox Signal* 25(5):233-251.

20. Kim CH, Kim JH, Xu J, Hsu CY, & Ahn YS (1999) Pyrrolidine dithiocarbamate induces bovine cerebral endothelial cell death by increasing the intracellular zinc level. *J Neurochem* 72(4):1586-1592.

21. Kim CH*, et al.* (2000) Biphasic effects of dithiocarbamates on the activity of nuclear factor-kappaB. *Eur J Pharmacol* 392(3):133-136.

22. Kojima R, Kamata, S. (1994) Zinc-selective membrane electrode using tetrabutyl thiuram disulfide neutral carrier. *Analytical Sciences* 10:409-412.

23. Prachayasittikul V, Prachayasittikul S, Ruchirawat S, & Prachayasittikul V (2013) 8-Hydroxyquinolines: a review of their metal chelating properties and medicinal applications. *Drug Des Devel Ther* 7:1157-1178.

24. Gamper N*, et al.* (2006) Oxidative modification of M-type K^+ channels as a mechanism of cytoprotective neuronal silencing. *EMBO J* 25(20):4996-5004.

25. Canzoniero LM, Manzerra P, Sheline CT, & Choi DW (2003) Membrane-permeant chelators can attenuate Zn2+-induced cortical neuronal death. *Neuropharmacology* 45(3):420-428.

26. Crouch PJ & Barnham KJ (2012) Therapeutic redistribution of metal ions to treat Alzheimer's disease. *Acc Chem Res* 45(9):1604-1611.

27. Telezhkin V, Reilly JM, Thomas AM, Tinker A, & Brown DA (2012) Structural requirements of membrane phospholipids for M-type potassium channel activation and binding. *J Biol Chem* 287(13):10001-10012.

28. Gamper N & Rohacs T (2012) Phosphoinositide sensitivity of ion channels, a functional perspective. *Subcell Biochem* 59:289-333.

29. Du X*, et al.* (2014) Control of somatic membrane potential in nociceptive neurons and its implications for peripheral nociceptive transmission. *Pain* 155(11):2306-2322.

30. Rose K*, et al.* (2011) Transcriptional repression of the M channel subunit Kv7.2 in chronic nerve injury. *Pain* 152(4):742-754.

31. Du X & Gamper N (2013) Potassium channels in peripheral pain pathways: expression, function and therapeutic potential. *Curr Neuropharmacol* 11(6):621-640.

32. Ooi L, Gigout S, Pettinger L, & Gamper N (2013) Triple cysteine module within M-type K^+ channels mediates reciprocal channel modulation by nitric oxide and reactive oxygen species. *J Neurosci* 33(14):6041-6046.

33. Krezel A, Hao Q, & Maret W (2007) The zinc/thiolate redox biochemistry of metallothionein and the control of zinc ion fluctuations in cell signaling. *Arch Biochem Biophys* 463(2):188-200.

34. Vallee BL & Falchuk KH (1993) The biochemical basis of zinc physiology. *Physiol Rev* 73(1):79-118.

35. Gamper N, Li Y, & Shapiro MS (2005) Structural requirements for differential sensitivity of KCNQ K^+ channels to modulation by Ca^{2+}/calmodulin. *Mol Biol Cell* 16:3538-3551.

36. Zaika O, Hernandez CC, Bal M, Tolstykh GP, & Shapiro MS (2008) Determinants within the turret and pore-loop domains of KCNQ3 K^+ channels governing functional activity. *Biophys J* 95(11):5121-5137.

37. Hernandez CC, Falkenburger B, & Shapiro MS (2009) Affinity for phosphatidylinositol 4,5-bisphosphate determines muscarinic agonist sensitivity of Kv7 K^+ channels. *J Gen Physiol* 134(5):437-448.

38. Hernandez CC, Zaika O, & Shapiro MS (2008) A carboxy-terminal inter-helix linker as the site of phosphatidylinositol 4,5-bisphosphate action on Kv7 (M-type) K^+ channels. *J Gen Physiol* 132(3):361-381.

39. Telezhkin V, Thomas AM, Harmer SC, Tinker A, & Brown DA (2013) A basic residue in the proximal C-terminus is necessary for efficient activation of the M-channel subunit Kv7.2 by $PI(4,5)P_2$. *Pflugers Arch*.

40. Iwasaki H*, et al.* (2008) A voltage-sensing phosphatase, Ci-VSP, which shares sequence identity with PTEN, dephosphorylates phosphatidylinositol 4,5-bisphosphate. *Proc Natl Acad Sci U S A* 105(23):7970-7975.

41. Falkenburger BH, Jensen JB, & Hille B (2010) Kinetics of PIP2 metabolism and KCNQ2/3 channel regulation studied with a voltage-sensitive phosphatase in living cells. *J Gen Physiol* 135(2):99-114.

42. Kruse M, Hammond GR, & Hille B (2012) Regulation of voltage-gated potassium channels by PI(4,5)P_2. *J Gen Physiol* 140(2):189-205.

43. Okamura Y, Murata Y, & Iwasaki H (2009) Voltage-sensing phosphatase: actions and potentials. *J Physiol* 587(3):513-520.

44. Stauffer TP, Ahn S, & Meyer T (1998) Receptor-induced transient reduction in plasma membrane PtdIns(4,5)P2 concentration monitored in living cells. *Curr Biol* 8(6):343-346.

45. Mavrantoni A*, et al.* (2015) A method to control phosphoinositides and to analyze PTEN function in living cells using voltage sensitive phosphatases. *Front Pharmacol* 6:68.

46. Wald T*, et al.* (2014) Quantification of potassium levels in cells treated with Bordetella adenylate cyclase toxin. *Anal Biochem* 450:57-62.

47. Zaydman MA*, et al.* (2013) Kv7.1 ion channels require a lipid to couple voltage sensing to pore opening. *Proc Natl Acad Sci U S A* 110(32):13180-13185.

48. Zhang Q*, et al.* (2013) Dynamic PIP_2 interactions with voltage sensor elements contribute to KCNQ2 channel gating. *Proc Natl Acad Sci U S A* 110(50):20093-20098.

49. Park KH*, et al.* (2005) Impaired KCNQ1-KCNE1 and phosphatidylinositol-4,5-bisphosphate interaction underlies the long QT syndrome. *Circ Res* 96(7):730-739.

50. Suh BC & Hille B (2007) Electrostatic interaction of internal Mg^{2+} with membrane PIP_2 Seen with KCNQ K^+ channels. *J Gen Physiol* 130(3):241-256.

51. Du X*, et al.* (2004) Characteristic interactions with phosphatidylinositol 4,5-bisphosphate determine regulation of kir channels by diverse modulators. *J Biol Chem* 279(36):37271-37281.

52. Linley JE, Pettinger L, Huang D, & Gamper N (2012) M channel enhancers and physiological M channel block. *J Physiol* 590(4):793-807.

53. Fukada T, Yamasaki S, Nishida K, Murakami M, & Hirano T (2011) Zinc homeostasis and signaling in health and diseases: Zinc signaling. *J Biol Inorg Chem* 16(7):1123-1134.

54. Bender K, Wellner-Kienitz MC, & Pott L (2002) Transfection of a phosphatidyl-4-phosphate 5-kinase gene into rat atrial myocytes removes inhibition of GIRK current by endothelin and alpha-adrenergic agonists. *FEBS Lett* 529(2-3):356-360.

55. Liu B*, et al.* (2010) The acute nociceptive signals induced by bradykinin in rat sensory neurons are mediated by inhibition of M-type K^+ channels and activation of Ca^{2+}-activated Cl^- channels. *J Clin Invest* 120(4):1240-1252.

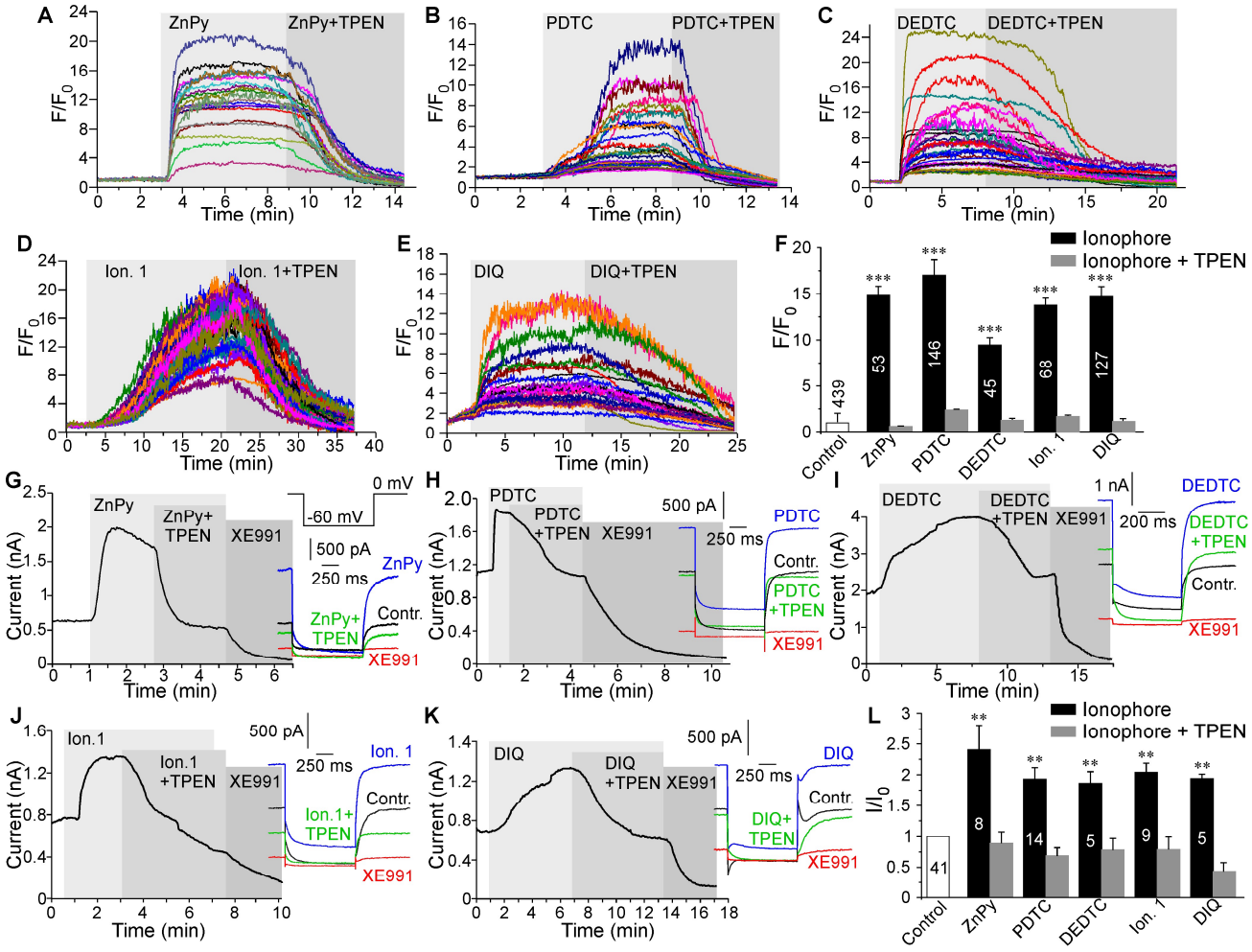
A
ZnPy
ZnPy+TPEN
F/F0
Time (min)
B
PDTC
PDTC+TPEN
C
DEDTC
DEDTC+TPEN
D
Ion. 1
Ion. 1+TPEN
E
DIQ
DIQ+TPEN
F
Ionophore
Ionophore + TPEN
439
53
146
45
68
127
Control
ZnPy
PDTC
DEDTC
Ion. 1
DIQ
G
ZnPy
ZnPy+ TPEN
XE991
0 mV
-60 mV
500 pA
250 ms
Current (nA)
Contr.
H
PDTC
PDTC +TPEN
I
DEDTC
DEDTC +TPEN
1 nA
200 ms
J
Ion.1
Ion.1 +TPEN
Ion.1+ TPEN
K
DIQ
DIQ +TPEN
DIQ+ TPEN
L
I/I0
41
8
14
5
9
5

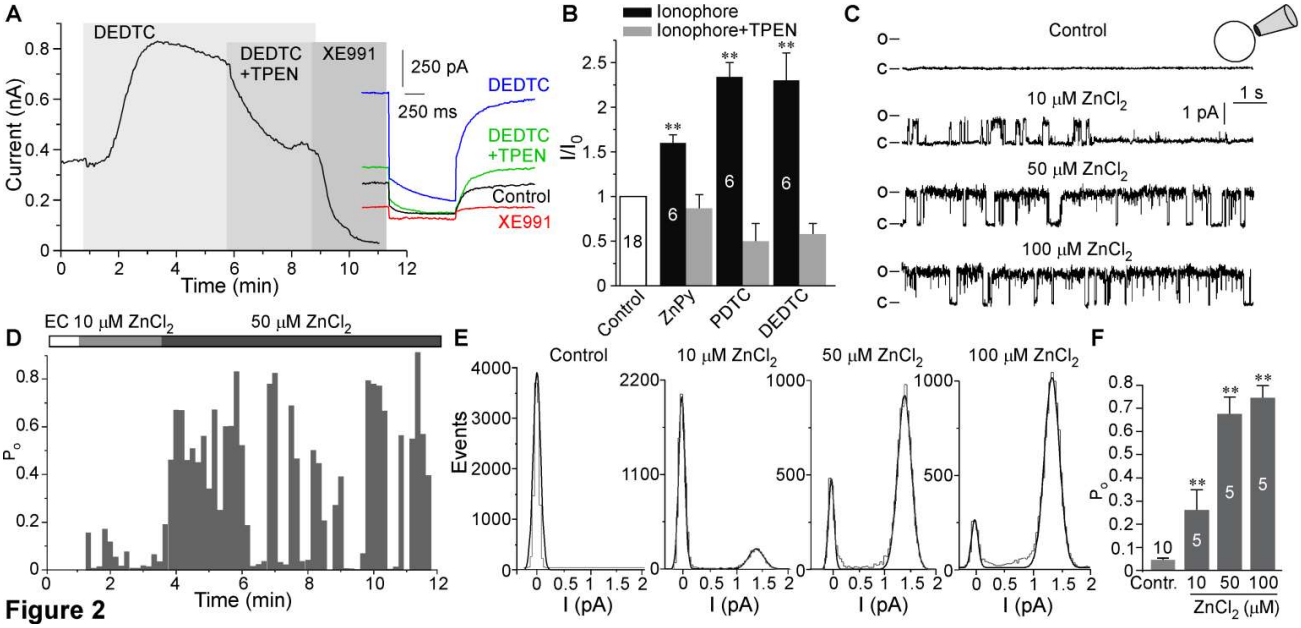
A
DEDTC
DEDTC +TPEN
XE991
250 pA
250 ms
DEDTC
DEDTC +TPEN
Control
XE991
Current (nA)
Time (min)
B
Ionophore
Ionophore+TPEN
I/I0
Control
ZnPy
PDTC
DEDTC
C
Control
10 μM ZnCl2
50 μM ZnCl2
100 μM ZnCl2
1 pA
1 s
D
EC 10 μM ZnCl2
50 μM ZnCl2
Po
Time (min)
E
Control
10 μM ZnCl2
50 μM ZnCl2
100 μM ZnCl2
Events
I (pA)
F
Po
Contr.
ZnCl2 (μM)

Figure 2

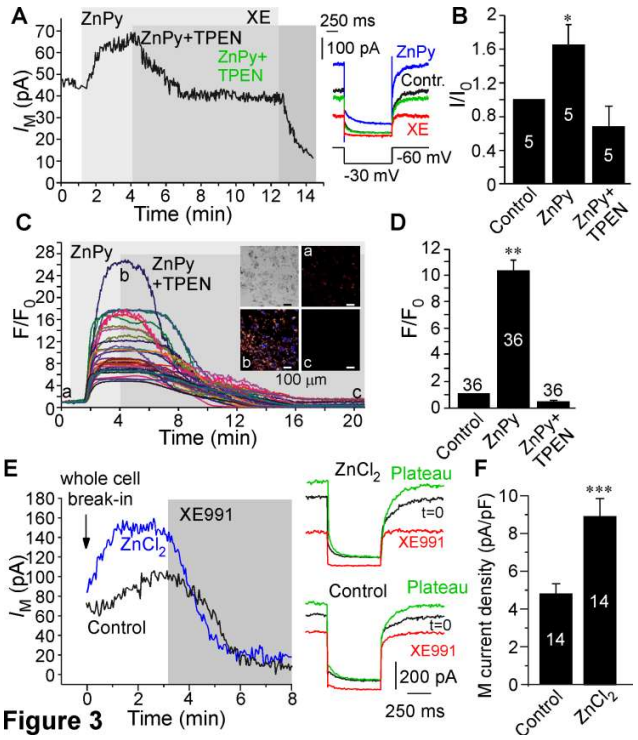
A
ZnPy
XE
ZnPy+TPEN
ZnPy+
TPEN
I_M (pA)
Time (min)
250 ms
100 pA
ZnPy
Contr.
XE
-60 mV
-30 mV
B
I/I_0
5
5
5
Control
ZnPy
ZnPy+
TPEN
C
ZnPy
ZnPy
+TPEN
F/F_0
a
b
c
100 μm
Time (min)
D
F/F_0
36
36
36
Control
ZnPy
ZnPy+
TPEN
E
whole cell
break-in
XE991
$ZnCl_2$
Control
I_M (pA)
Time (min)
$ZnCl_2$
Plateau
t=0
XE991
Control
Plateau
t=0
XE991
200 pA
250 ms
F
M current density (pA/pF)
14
14
Control
$ZnCl_2$

Figure 3

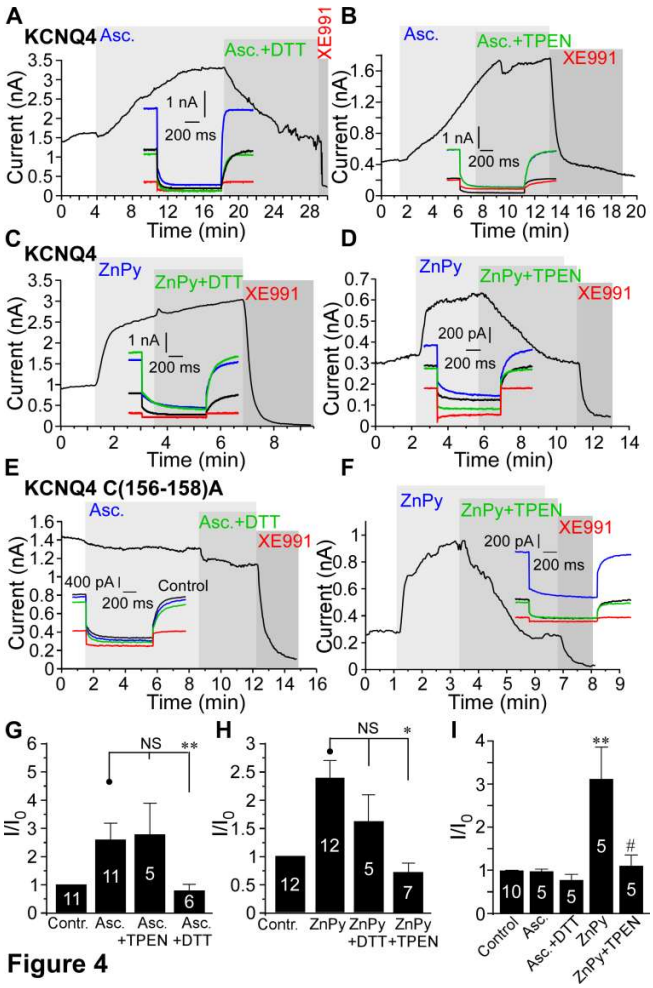
A
KCNQ4
Asc.
Asc.+DTT
XE991
Current (nA)
1 nA
200 ms
Time (min)
B
Asc.
Asc.+TPEN
XE991
1 nA
200 ms
Time (min)
C
KCNQ4
ZnPy
ZnPy+DTT
XE991
1 nA
200 ms
Time (min)
D
ZnPy
ZnPy+TPEN
XE991
200 pA
200 ms
Time (min)
E
KCNQ4 C(156-158)A
Asc.
Asc.+DTT
XE991
400 pA
200 ms
Control
Time (min)
F
ZnPy
ZnPy+TPEN
XE991
200 pA
200 ms
Time (min)
G
I/I0
NS
**
11
5
6
Contr.
Asc.
Asc. +TPEN
Asc. +DTT
H
I/I0
NS
*
12
5
7
Contr.
ZnPy
ZnPy +DTT+TPEN
I
I/I0
**
#
10
5
5
5
Control
Asc.
Asc.+DTT
ZnPy
ZnPy+TPEN

Figure 4

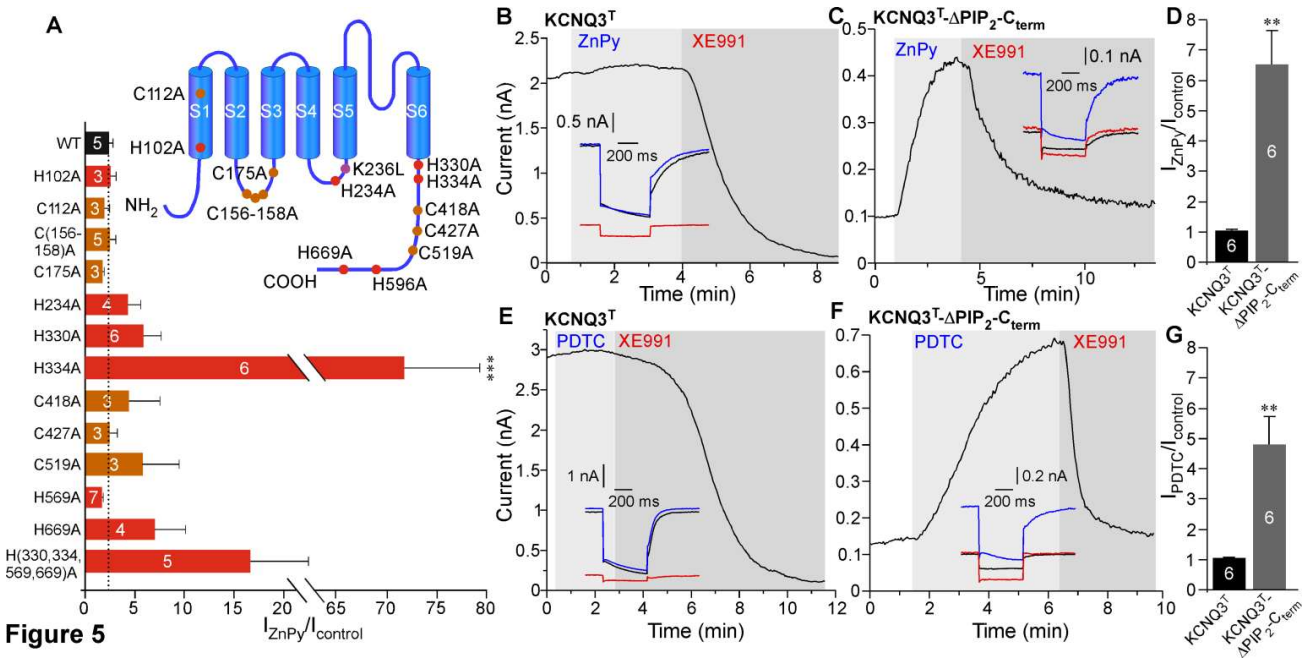
A
C112A
S1
S2
S3
S4
S5
S6
H102A
C175A
K236L
H330A
H334A
H234A
NH2
C156-158A
C418A
C427A
C519A
H669A
COOH
H596A
WT
H102A
C112A
C(156-158)A
C175A
H234A
H330A
H334A
C418A
C427A
C519A
H569A
H669A
H(330,334,569,669)A
***
IZnPy/Icontrol
B
KCNQ3T
ZnPy
XE991
0.5 nA
200 ms
Current (nA)
Time (min)
C
KCNQ3T-ΔPIP2-Cterm
ZnPy
XE991
0.1 nA
200 ms
Time (min)
D
**
IZnPy/Icontrol
KCNQ3T
KCNQ3T-ΔPIP2-Cterm
E
KCNQ3T
PDTC
XE991
1 nA
200 ms
Current (nA)
Time (min)
F
KCNQ3T-ΔPIP2-Cterm
PDTC
XE991
0.2 nA
200 ms
Time (min)
G
**
IPDTC/Icontrol
KCNQ3T
KCNQ3T-ΔPIP2-Cterm

Figure 5

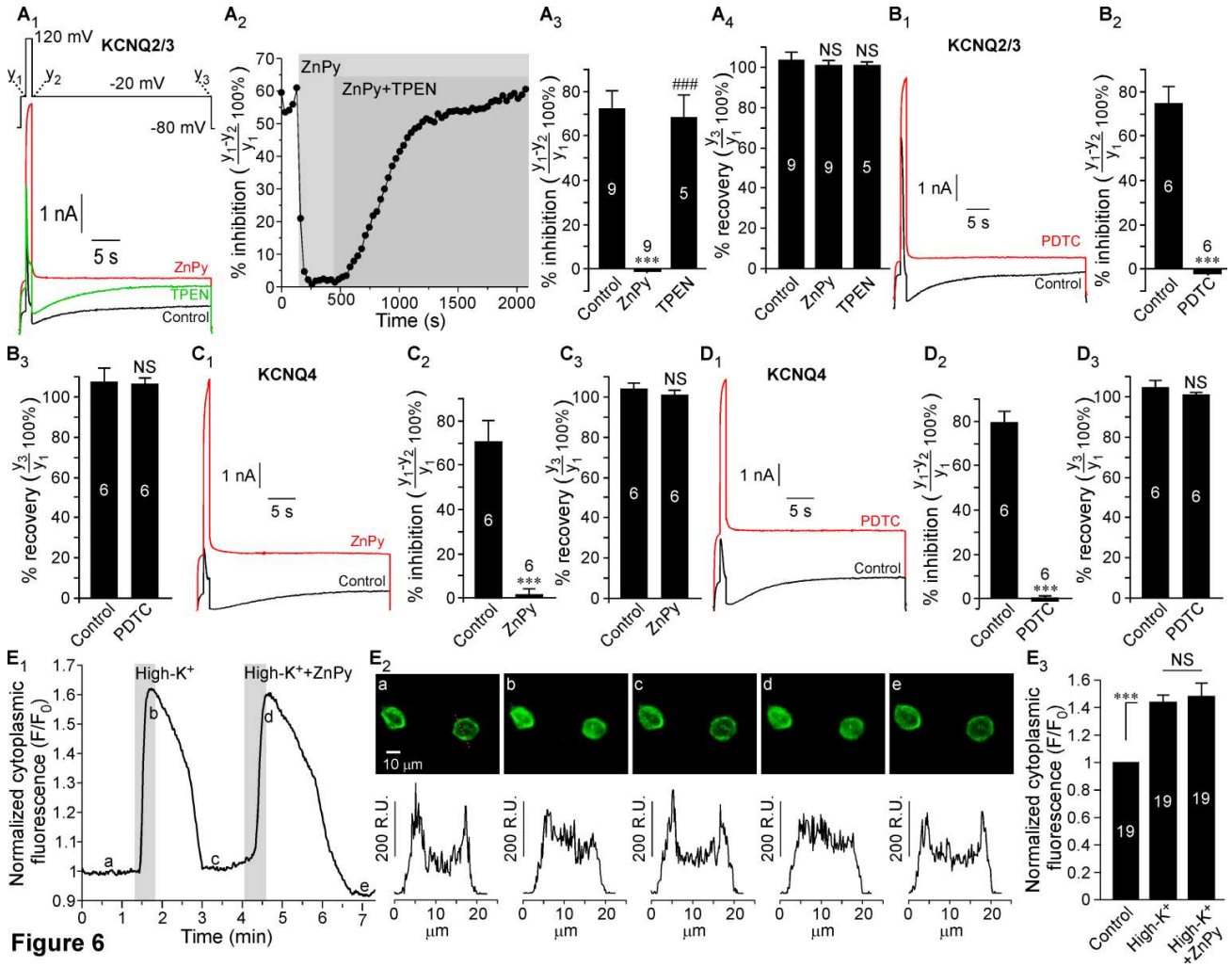
A1
120 mV
KCNQ2/3
y1
y2
-20 mV
y3
-80 mV
1 nA
5 s
ZnPy
TPEN
Control
A2
ZnPy
ZnPy+TPEN
% inhibition ((y1-y2)/y1 100%)
Time (s)
A3
% inhibition ((y1-y2)/y1 100%)
###
***
Control
ZnPy
TPEN
A4
% recovery (y3/y1 100%)
NS
Control
ZnPy
TPEN
B1
KCNQ2/3
1 nA
5 s
PDTC
Control
B2
% inhibition ((y1-y2)/y1 100%)
***
Control
PDTC
B3
% recovery (y3/y1 100%)
NS
Control
PDTC
C1
KCNQ4
1 nA
5 s
ZnPy
Control
C2
% inhibition ((y1-y2)/y1 100%)
***
Control
ZnPy
C3
% recovery (y3/y1 100%)
NS
Control
ZnPy
D1
KCNQ4
1 nA
5 s
PDTC
Control
D2
% inhibition ((y1-y2)/y1 100%)
***
Control
PDTC
D3
% recovery (y3/y1 100%)
NS
Control
PDTC
E1
Normalized cytoplasmic fluorescence (F/F0)
High-K+
High-K++ZnPy
a
b
c
d
e
Time (min)
E2
10 μm
200 R.U.
μm
E3
Normalized cytoplasmic fluorescence (F/F0)
***
NS
Control
High-K+
High-K+ +ZnPy

Figure 6

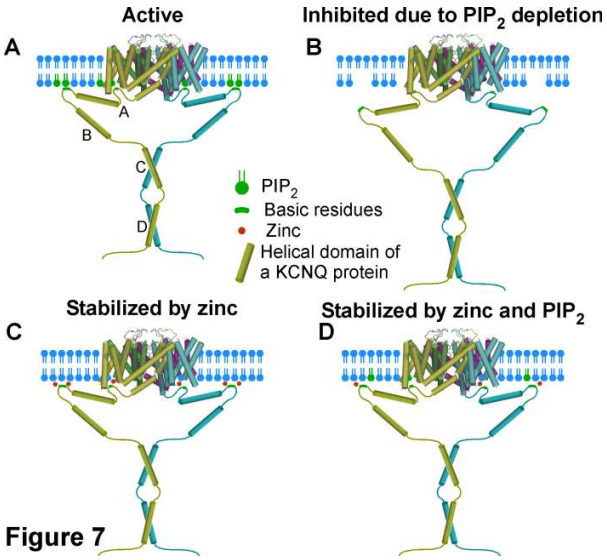
Active
Inhibited due to PIP2 depletion
A
B
A
B
C
D
PIP2
Basic residues
Zinc
Helical domain of
a KCNQ protein
Stabilized by zinc
Stabilized by zinc and PIP2
C
D

Figure 7

Zinc pyrithione (ZnPy)

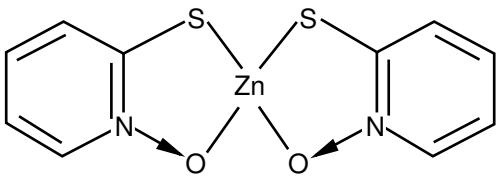

5,7-Diiodo-8-hydroxyquinoline (DIQ)

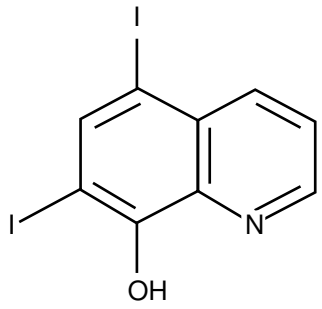

Zinc diethyldithiocarbamate (Zn-DEDTC)

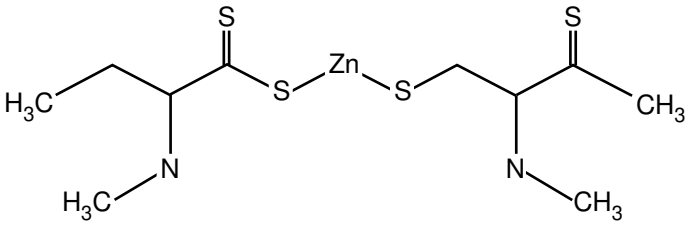

Ammonium pyrrolidinedithiocarbamate (PDTC)

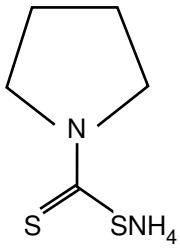

Tetrabutylthiuram disulfide (zinc ionophore I)

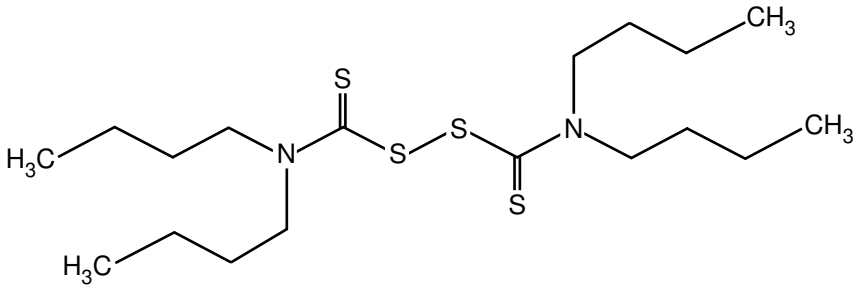

Figure S1

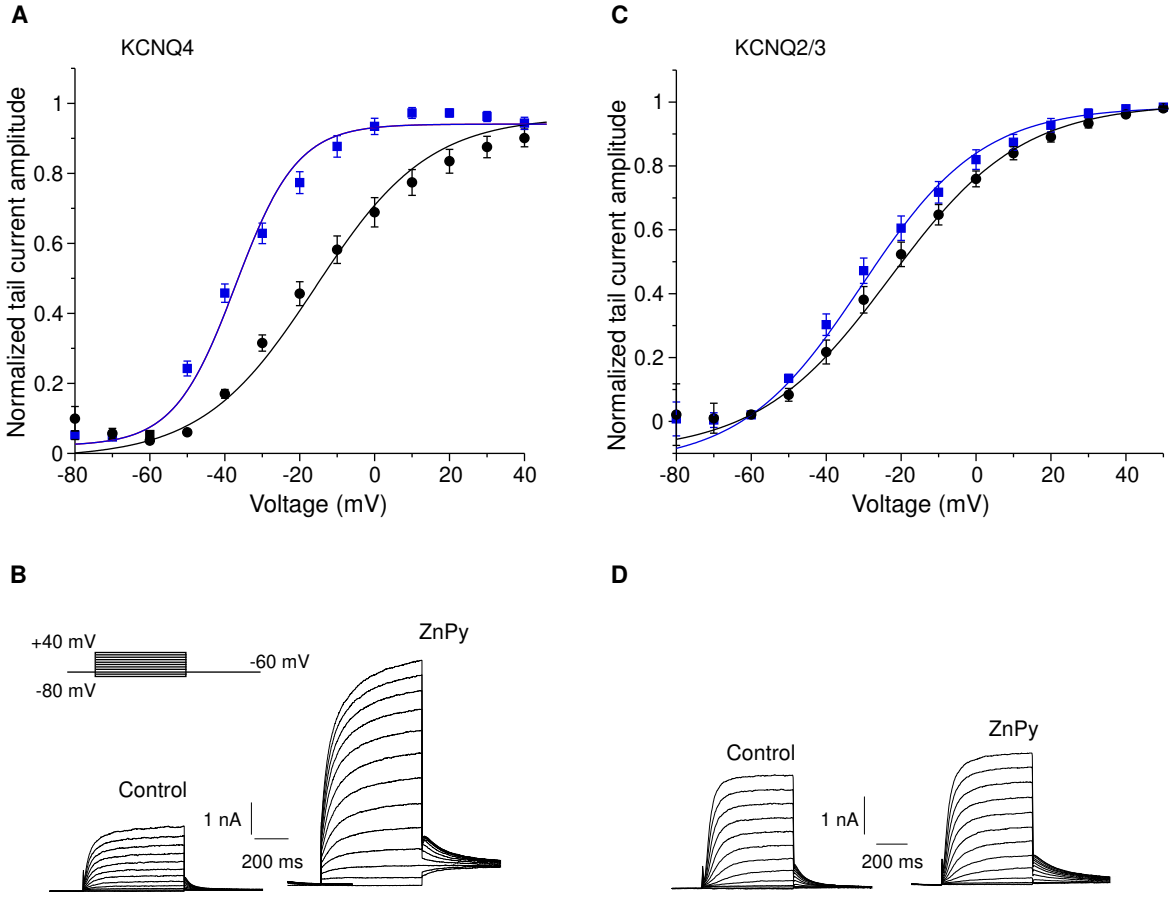
A
KCNQ4
Normalized tail current amplitude
Voltage (mV)
C
KCNQ2/3
Normalized tail current amplitude
Voltage (mV)
B
+40 mV
-60 mV
-80 mV
ZnPy
Control
1 nA
200 ms
D
Control
ZnPy
1 nA
200 ms

Figure S2

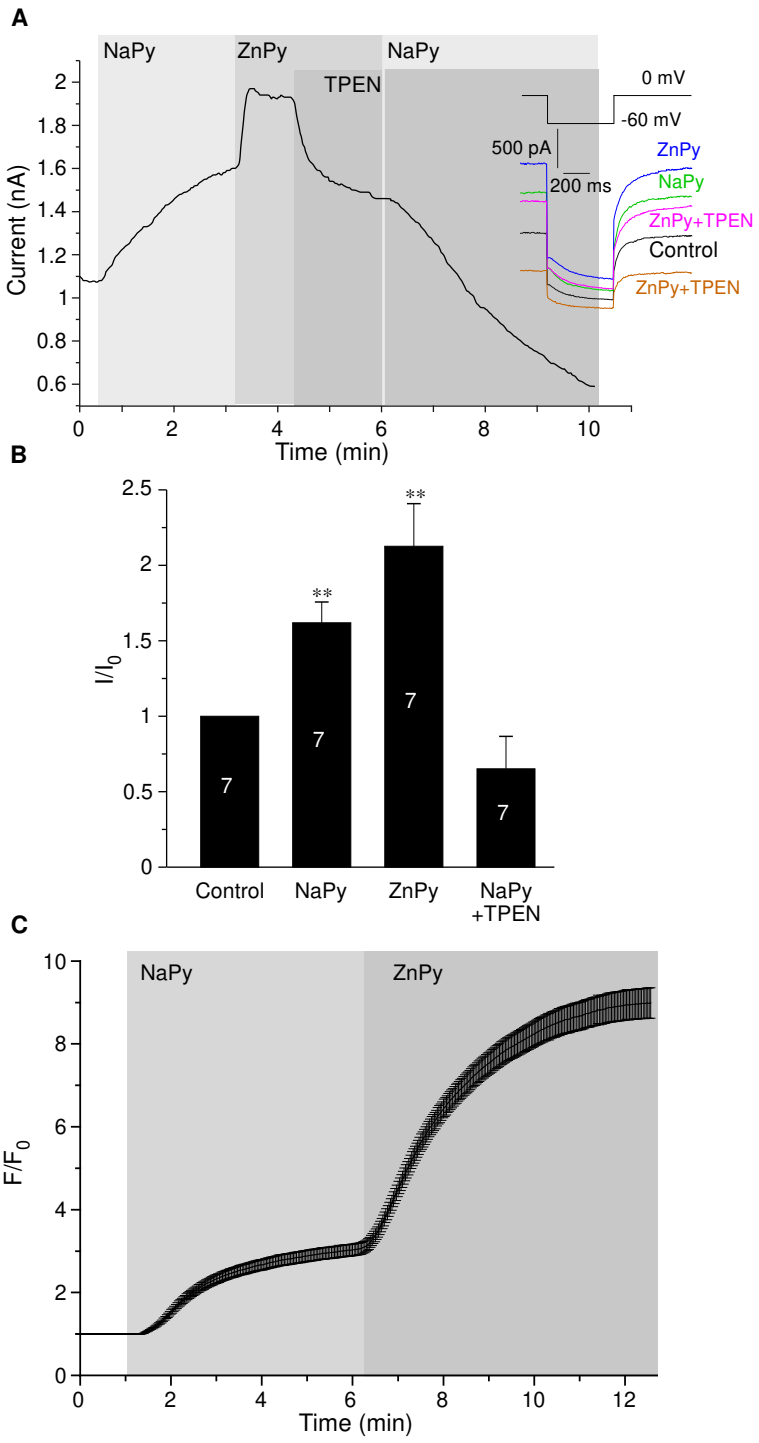
A
NaPy
ZnPy
NaPy
TPEN
Current (nA)
Time (min)
0 mV
-60 mV
500 pA
200 ms
ZnPy
NaPy
ZnPy+TPEN
Control
ZnPy+TPEN
B
I/I0
Control
NaPy
ZnPy
NaPy +TPEN
**
**
7
7
7
7
C
NaPy
ZnPy
F/F0
Time (min)

Figure S3

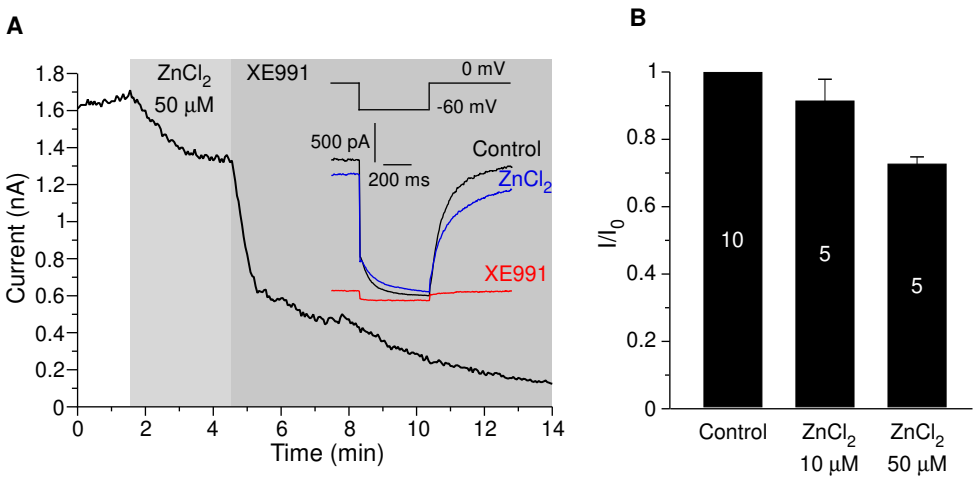
A
B
ZnCl2
50 µM
XE991
0 mV
-60 mV
500 pA
200 ms
Control
ZnCl2
XE991
Current (nA)
Time (min)
I/I0
10
5
5
Control
ZnCl2
10 µM
ZnCl2
50 µM

Figure S4

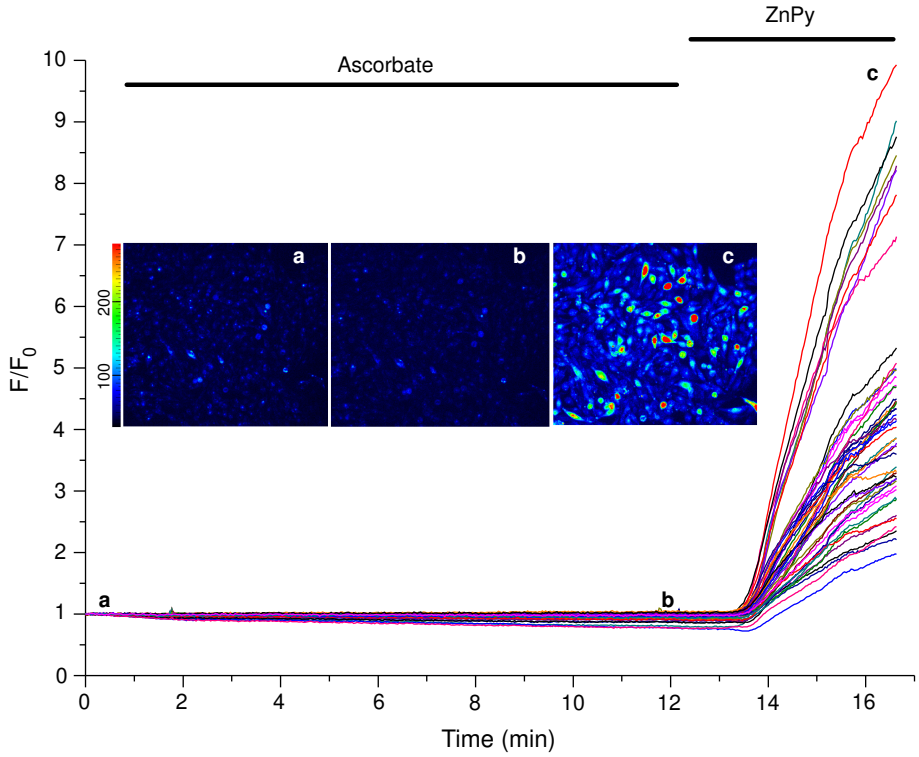
ZnPy
Ascorbate
c
a
b
c
200
100
a
b
F/F0
Time (min)
0
1
2
3
4
5
6
7
8
9
10
0
2
4
6
8
10
12
14
16

Figure S5

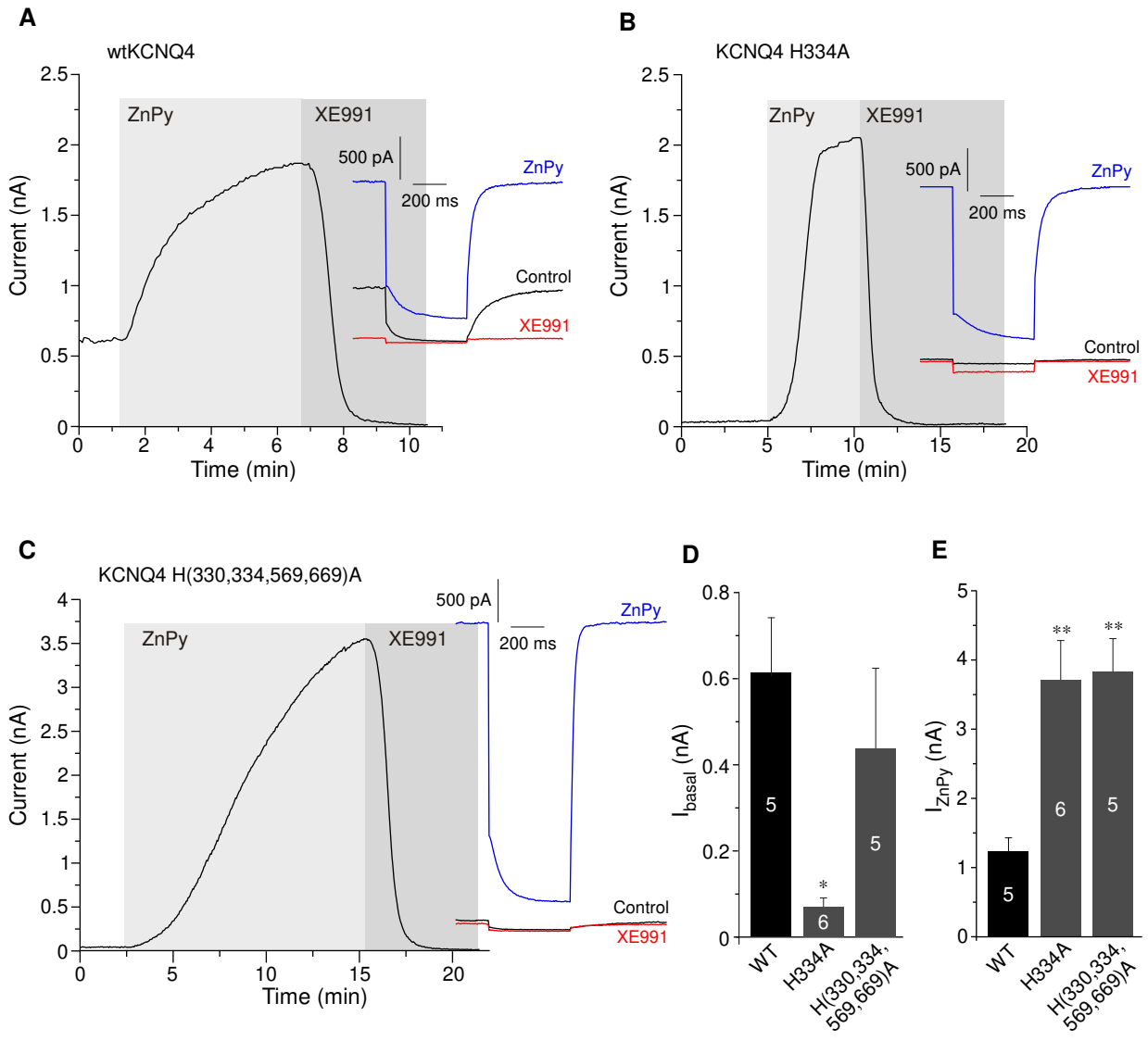
A
wtKCNQ4
ZnPy
XE991
500 pA
200 ms
ZnPy
Control
XE991
Current (nA)
Time (min)
B
KCNQ4 H334A
ZnPy
XE991
500 pA
200 ms
ZnPy
Control
XE991
Current (nA)
Time (min)
C
KCNQ4 H(330,334,569,669)A
ZnPy
XE991
500 pA
200 ms
ZnPy
Control
XE991
Current (nA)
Time (min)
D
I_{basal} (nA)
WT
H334A
H(330,334, 569,669)A
E
I_{ZnPy} (nA)
WT
H334A
H(330,334, 569,669)A

Figure S6

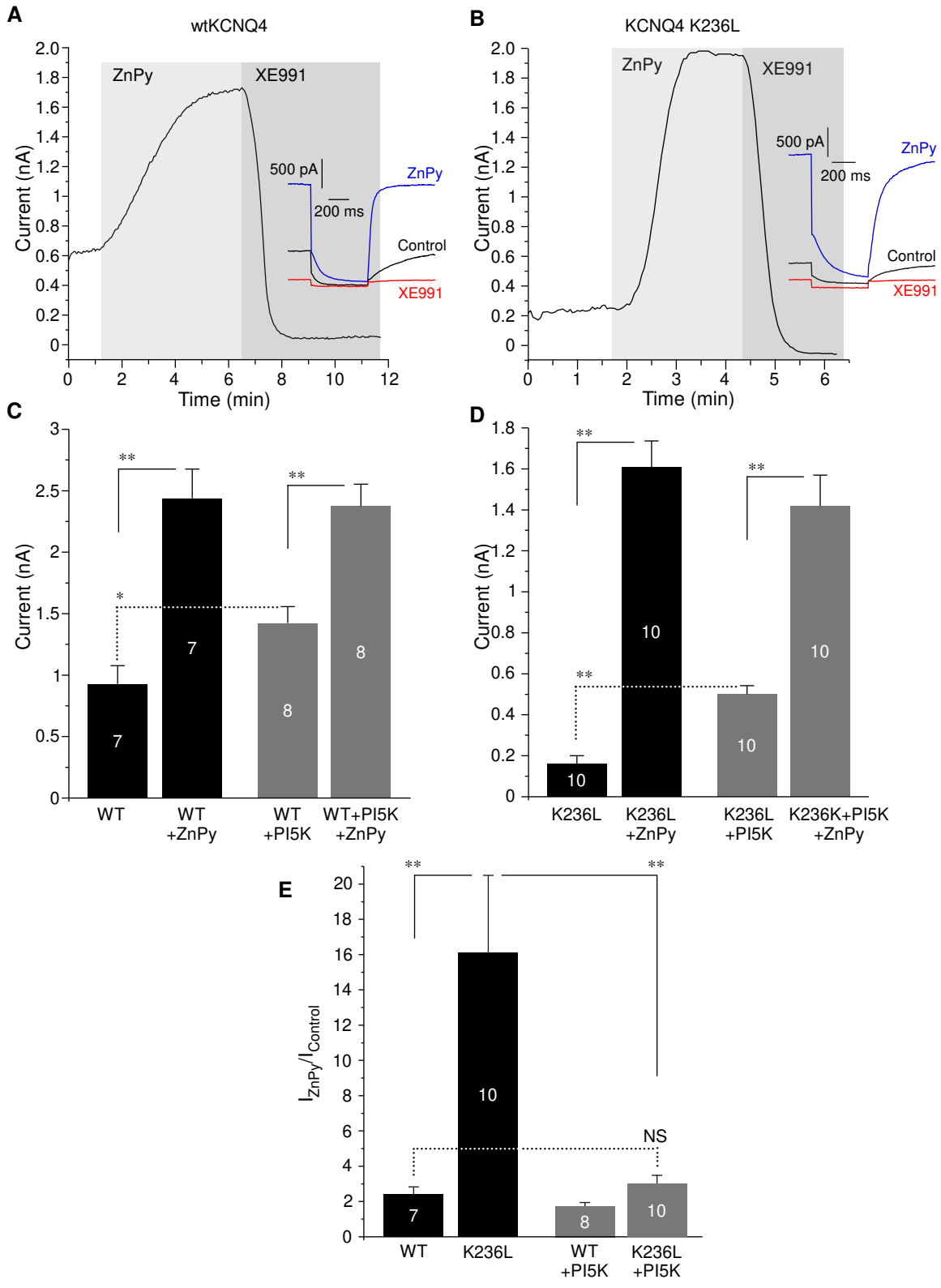
A
wtKCNQ4
ZnPy
XE991
500 pA
200 ms
ZnPy
Control
XE991
Current (nA)
Time (min)
B
KCNQ4 K236L
ZnPy
XE991
500 pA
200 ms
ZnPy
Control
XE991
Current (nA)
Time (min)
C
Current (nA)
WT
WT +ZnPy
WT +PI5K
WT+PI5K +ZnPy
D
Current (nA)
K236L
K236L +ZnPy
K236L +PI5K
K236K+PI5K +ZnPy
E
I_ZnPy/I_Control
NS
WT
K236L
WT +PI5K
K236L +PI5K

Figure S7

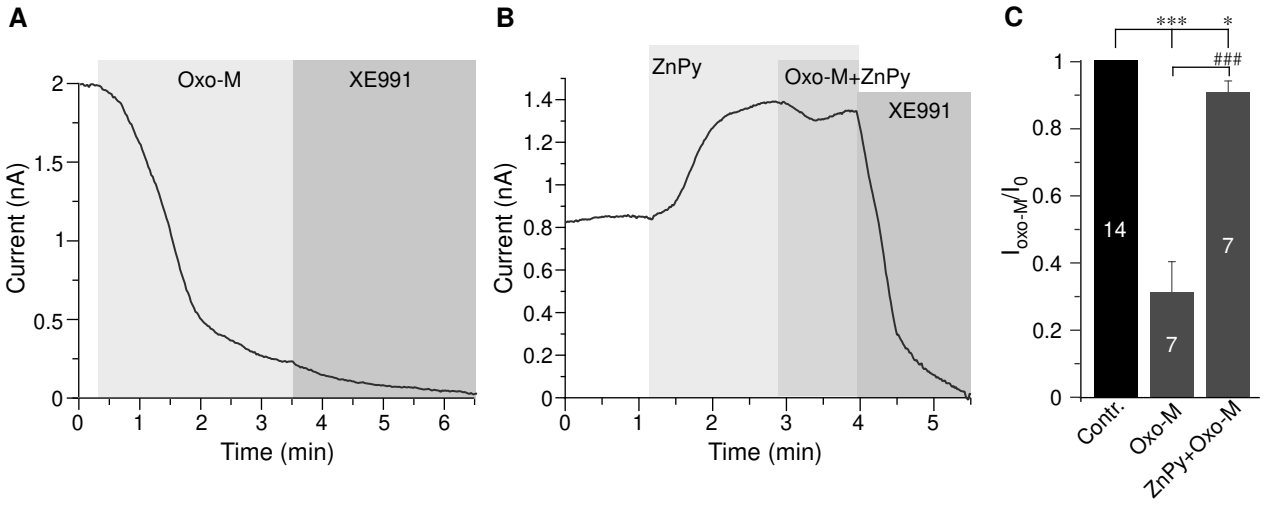
A
Oxo-M
XE991
Current (nA)
Time (min)
B
ZnPy
Oxo-M+ZnPy
XE991
Current (nA)
Time (min)
C
***
*
###
14
7
7
Contr.
Oxo-M
ZnPy+Oxo-M

Figure S8

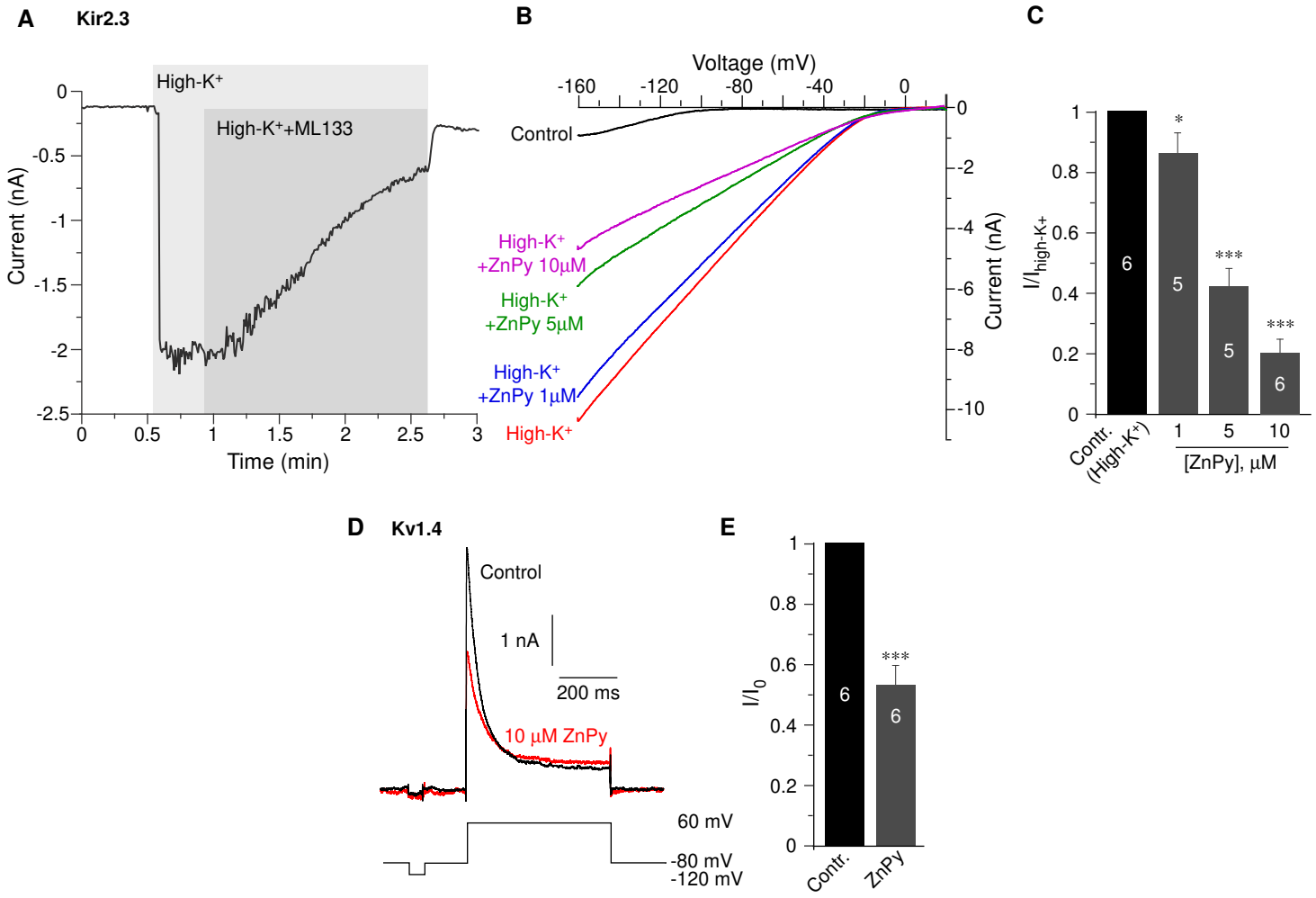
A
Kir2.3
High-K+
High-K+ +ML133
Current (nA)
Time (min)
B
Voltage (mV)
Control
High-K+ +ZnPy 10µM
High-K+ +ZnPy 5µM
High-K+ +ZnPy 1µM
High-K+
Current (nA)
C
I/I high-K+
Contr. (High-K+)
[ZnPy], µM
D
Kv1.4
Control
1 nA
200 ms
10 µM ZnPy
60 mV
-80 mV
-120 mV
E
I/I0
Contr.
ZnPy

Figure S9

Supplemental Figure legends.

Figure S1. Chemical structure of zinc ionophores used.

Figure S2. Effect of zinc pyrithione (ZnPy; 10 μM) on the voltage dependence of KCNQ4 (**A**, **B**) and KCNQ2/3 (**C**, **D**) channels expressed in CHO cells. Voltage protocol is depicted in the inset in (**B**). Tail current amplitudes measured within first 5 ms of the final voltage step to -60 mV were plotted against main step voltage and fitted with Boltzmann function (**A**, **C**). Example current traces are shown in (**B**, **D**).

Figure S3. Sodium pyrithione augments KCNQ4 current by raising intracellular zinc. (**A**) Perforated patch clamp recordings from the KCNQ4-transfected CHO cells showing the time courses for effects of 10 μM sodium pyrithione (NaPy), 10 μM ZnPy and 20 μM TPEN (as labelled) on the KCNQ4 current amplitude. Example current traces are shown on the right; voltage protocol is given in inset above the traces. (**B**) Summary of the experiments presented in (**A**); number of cells is indicated within the bars; asterisks indicate significant difference from the baseline with **p<0.01 (paired t-test). (**C**) Fluorescence imaging of CHO cells loaded with zinc fluorophore, FluoZin^{TM}-3AM. Mean time course of changes in FluoZin-3 fluorescence during application of 10 μM NaPy followed by 10 μM ZnPy; n=31.

Figure S4. Extracellularly applied zinc does not augment KCNQ4 current. (**A**) Perforated patch clamp recording from the KCNQ4-transfected CHO cells showing the time courses for effects of 50 μM $ZnCl_2$ and 10 μM XE991 (as labelled) on the KCNQ4 current amplitude. Example current traces are shown in the inset; voltage protocol is given in the inset above the traces. (**B**) Summary of the experiments as these presented in (**A**); number of cells is indicated within the bars.

Figure S5. Ascorbate does not produce measurable increase of intracellular zinc levels. Fluorescence imaging of CHO cells loaded with zinc fluorophore, FluoZin^{TM}-3AM. Shown are the example time courses of changes in FluoZin-3 fluorescence during application of 2 mM ascorbate

and 10 μM ZnPy (as labelled). Example fluorescence micrographs taken at the times indicated by the letters are shown in the inset.

Figure S6. Replacement of C-terminal histidines in KCNQ4 increases the current potentiation efficacy of zinc. Perforated patch clamp recordings from the CHO cells transfected with the wtKCNQ4 (**A**), KCNQ4 H334A (**B**) or KCNQ4 H(330,334,569,669)A (**C**) showing the effects of 10 μM ZnPy and 10 μM XE991 (as labelled) on the current amplitude. Example current traces are shown in the insets. Summaries of baseline current amplitudes and maximal ZnPy-induced current amplitudes (both measured at 0 mV) for the wtKCNQ4 and two mutants are shown in (**D**) and (**E**), respectively. Number of cells is indicated within the bars; asterisks indicate significant difference from the wtKCNQ4 with *p<0.05 or **p<0.01 (one-way ANOVA with Bonferroni correction).

Figure S7. Neutralization of a PIP_2-interacting residue in the S4-S5 linker of KCNQ4 increases channel PIP_2 dependence and current potentiation efficacy of zinc. Perforated patch clamp recordings from the CHO cells transfected with the wtKCNQ4 (**A**) or KCNQ4 K236L (**B**) showing the effects of 10 μM ZnPy and 10 μM XE991 (as labelled) on the current amplitude. Example current traces are shown in the insets. Panels (**C**, **D**) show summaries of baseline current amplitudes and maximal ZnPy-induced current amplitudes (both measured at 0 mV) for the wtKCNQ4 (**C**) or KCNQ4 K236L (**D**) overexpressed either alone or together with the PI(4)5-kinase (PI5K). Panel (**E**) summarizes the augmenting effect of ZnPy (normalized to baseline) for wtKCNQ4 or KCNQ4 K236L in CHO cells with or without PI(4)5-kinase co-expression (as labelled). Asterisks denote significant difference from the group indicated by the line connector with *p<0.05 or **p<0.01 (one-way ANOVA with Bonferroni correction).

Figure S8. ZnPy reduces inhibition of Kv7.4 by M1 muscarinic receptor activation. (**A**) Perforated patch clamp recording from the KCNQ4-transfected CHO cells showing the time courses for effects of 20 μM Oxotremorine-M (Oxo-M) and 10 μM XE991 (as labelled) on the KCNQ4 current amplitude. (**B**) Is similar to (**A**) but 10 μM ZnPy was applied before Oxo-M. (**C**) Summary

of the experiments as these presented in (**A, B**); number of cells is indicated within the bars. Asterisks and number symbols denote significant difference from the group indicated by the line connector with $p<0.05$, $p<0.001$ (paired or unpaired t-test, as appropriate).

Figure S9. Effects of ZnPy on Kir2.3 and Kv1.4. (**A-C**) Effect of ZnPy on Kir2.3; (**A**) Whole-cell patch clamp recording from the HEK293 cells transfected with Kir2.3 (kind gift from Diomedis Logothetis, Virginia Commonwealth University School of Medicine) and GFP showing the time courses of the effect of 30 μM of Kir channel inhibitor, ML133 on the Kir2.3 current amplitude. Currents were recorded by 250 ms voltage ramps from -160 to +20 mV from a holding potential of 0 mV in response to application of 'high-K^+ solution' of the following composition (in mM): NaCl 5, KCl 140, $CaCl_2$ 2, $MgCl_2$ 1, HEPES 20 and Glucose 10, (pH 7.4 with NaOH). Control bath solution contained (in mM): NaCl 160, KCl 2.5, $CaCl_2$ 2, $MgCl_2$ 1, HEPES 10, and Glucose 8, (pH 7.4 with NaOH). The intracellular solution contained (in mM): KCl 175, $MgCl_2$ 5, HEPES 5, BAPTA 0.1, K_2ATP 3 and NaGTP 0.1 (pH 7.2 with KOH). (**B**) Example traces showing effects of ZnPy (1-10 μM) on Kir2.3 currents recorded as in (**A**). (**C**) Summary of the experiments as presented in (**B**); maximal inward current amplitude at -160 mV is analysed. Number of cells is indicated within the bars. Asterisks denote significant difference from the control with $p<0.05$, $p<0.001$ (Repeated measures ANOVA). (**D**, **E**) Effect of ZnPy on Kv1.4; (**D**) Exemplary current traces recorded using whole-cell patch clamp from the HEK293 cells transfected with Kv1.4 (Youbio, China) and GFP in control conditions and in the presence of 10 μM ZnPy; voltage protocol is depicted below the traces. Recording solutions were as follows. The external solution contained (in mM): NaCl 140, KCl 5.4, $CaCl_2$ 2, $MgCl_2$ 1.0, HEPES 10 and glucose 10 (pH 7.3 with NaOH); intracellular solution contained (in mM): KCl 140, Mg-ATP 4, $MgCl_2$ 1, $CaCl_2$ 1 and HEPES 10 (pH 7.4 with KOH). (**E**) Summary of the experiments as in (**D**); number of cells is indicated within the bars. Asterisks denote significant difference from the control with $p<0.001$ (paired t-test).